Comparitive study of Quantum Phase Estimation on a simple Pairing Hamiltonian.

Heine Aabø og Stian Bilek

June 2019

Abstract

Our aim in this study was to implement a quantum algorithm for estimating the eigenvalues of a pairing hamiltonian and comparing the found eigenvalues with the benchmark provided by using Full Configuration Interaction theory (FCI). Coupled Cluster Doubles (CCD) was also implemented to provide a comparison with a popular and computational efficient method. We found that the results provided by FCI was within two standard deviations of the eigenvalues found with the quantum phase estimation algorithm. We got the eigenvalues -0.6 ± 0.1 and 1.61 ± 0.06 for one pair, and this result is consistent with the FCI eigenvalues -0.618 and 1.618. For two pairs, the quantum algorithm yielded 1.0 ± 0.2 which also is consistent with the FCI eigenvalue of 1.0. With CCD, our results matched perfectly with FCI for one pair. For two pairs however, our results diverged as we increased the number of spin orbitals. We argued that even though CCD should be able to account for all excitations, it lacks the degrees of freedom provided by FCI.

1 Introduction

Feynman noted in 1982 that calculating properties of an arbitrary quantum system on a classical device is a seemingly very inefficient thing to do [7]. It is a problem which scales exponentially with the number of particles in the model being simulated, meaning that for complex molecules like for example the caffeine molecule, current modelling approaches is at their limits. He suggested that a quantum device might be able to calculate such properties efficiently, meaning that the problem instead scales polynomially with the number of particles. In 1985, David Deutch provided a description of such a quantum device, namely an universal quantum computer [4]. Moving forward to 1996, American physicist Seth Lloyd indeed showed that such a computer could simulate quantum systems efficiently [8]. In the absence of quantum computers, several classical approximation methods have been developed, for example Full Configuration Interaction (FCI). While this method provides an exact solution within a single particle basis, it indeed doesn't scale well with the problem size. Hence truncated Coupled Cluster schemes are favored, sacrificing precision for scalability.

Today, Quantum computers have moved beyond pen and paper and there are several big companies working on making these devices a reality, including IBM and Google. IBM even

has a quantum computer consisting of 16 qubits (the quantum equivalent of classical bits), which can be accessed and programmed over the cloud. There are, however, still a lot of hurdles that has to be dealt with in order to make these devices useful in practice. Measurement noise and gate noise are among some of them [11]. Fortunately, we can run small scale experiments by simulating quantum computers on our classical hardware.

In this study, our aim is to implement the phase estimation quantum algorithm, described in [10], to approximate the eigenvalues of the pairing hamiltonian. We will make use of IBM's python library "qiskit" to write the code in python and run the code by using IBM's quantum computer simulator. The found eigenvalues will be compared with the eigenvalues calculated with Full Configuration Interaction theory as these eigenvalues will be exact within the subspace spanned by our basis states. We will also run the same quantum algorithm on a simulation of a noisy quantum computer by setting some gate and measurement properties gathered from IBM's real quantum computer (Melbourne). Coupled Clusted Doubles (CCD) will also be evaluated on the same system, as it enables us to compare the golden standard in quantum chemistry with a promising Quantum algorithm. The theory section should contain the basic building blocks for understanding the quantum algorithms we utilized and also the theory behind FCI and CCD. [9] is a recommended read for a wider understanding of the quantum computing concepts. The code used to produce our results for the Phase estimation algorithm can be found at:
`https://github.com/stiandb/QuantumComputing`.
The implementation of the CCD code can be found at:
`https://github.com/heineaabo/CCD-Pairing-model`.

Contents

2 Theory

2.1 Second Quantization

When we study systems of fermions a common practice is to assume that the wave function can be approximated as the anti-symmetric Slater determinant. Slater determinants are useful as they lead to a straightforward implementation of the Pauli principle where no two particles can be in the same state or at the same place. Since it is anti-symmetric, a change in sign will be induced upon interchanging two particles. Given n occupied single-particle orbitals ϕ, this can be written as

$$|\Phi\rangle = \frac{1}{\sqrt{n!}} \begin{vmatrix} \phi_1(x_1) & \dots & \phi_1(x_n) \\ \vdots & & \vdots \\ \phi_n(x_1) & \dots & \phi_n(x_n) \end{vmatrix} \tag{1}$$

without any notation of what orbitals are occupied or not. To develop an organized notation we start by introducing the vacuum state, being the state of a system with no particles $|\rangle$. If we denote occupied single-particle orbitals with $i, j, \dots$, we can create a particle in our vacuum by acting on it with a creation operator

$$a_i^\dagger |\rangle = |i\rangle \tag{2}$$

and remove it by acting with an annihilation operator.

$$a_i |i\rangle = |\rangle \tag{3}$$

The Slater determinant can be defined as a series of creation operators acting on the vacuum state

$$|\Phi_0\rangle = \prod_{i=1}^{n} a_i^\dagger \, |\rangle \tag{4}$$

where $|\Phi_0\rangle$ now contains all orbitals under the Fermi level, and we will refer to this state as our reference vacuum. The Fermi level is defined as the level under which all lowest possible orbitals are occupied. Next we introduce the concept of virtual orbitals which we will label $a, b, \ldots$, furthermore $i, j, \ldots$ will denote the occupied single-particle orbitals. To excite a particle we then have to remove an occupied orbital and replace it with a virtual orbital.

$$a_a^\dagger a_i \, |\Phi_0\rangle = |\Phi_i^a\rangle \tag{5}$$

We can regard this as creating both a hole state and a particle state. And so both $a_a^\dagger$ and a_i are creation operators, leaving a_a and $a_i^\dagger$ as annihilation operators. Throughout this article we will label particle states $a, b, \ldots$ and hole states $i, j, \ldots$ when we deal with states and operators.

2.1.1 Hamiltonian

The electronic Hamiltonian in second quantized form is

$$\hat{H} = \sum_{pq} \langle p| \, \hat{h} \, |q\rangle \, a_p^\dagger a_q + \frac{1}{4} \sum_{pqrs} \langle pq| \, \hat{v} \, |rs\rangle \, a_p^\dagger a_q^\dagger a_s a_r \tag{6}$$

where the indices run over all orbitals of interest. With this Hamiltonian we are dealing with non-commuting creation and annihilation operators, and so a common practice is to normal order these. Normal ordering means having all annihilation operators to the right of all creation operators. First we refresh our memory of the anti-commutation rules of creation and annihilation operators

$$a_n a_m + a_m a_n = a_n^\dagger a_m^\dagger + a_m^\dagger a_n^\dagger = 0, \qquad a_n a_m^\dagger + a_m^\dagger a_n = \delta_{mn} \tag{7}$$

This means that for particle states we have

$$a_a a_b^\dagger + a_b^\dagger a_a = \delta_{ab}$$

and for hole states we have

$$a_i^\dagger a_j + a_j a_i^\dagger = \delta_{ij}$$

We can then define the contraction between operators as

$$\overbrace{a_n a_m^\dagger} = a_n a_m^\dagger - \{a_n a_m^\dagger\}_N \tag{8}$$

where $\{\ \}_N$ means the normal ordered form. For particle and hole states the only non-zero contractions are

$$\overbrace{a_a a_b^\dagger} = a_a a_b^\dagger - \{a_a a_b^\dagger\}_N = a_a a_b^\dagger + a_b^\dagger a_a = \delta_{ab} \tag{9}$$

$$\overbrace{a_i^\dagger a_j} = a_i^\dagger a_j - \{a_i^\dagger a_j\}_N = a_i^\dagger a_j + a_j a_i^\dagger = \delta_{ij} \tag{10}$$

Looking at the first term in our Hamiltonian we need to normal order $\sum_{pq} a_p^\dagger a_q$. Using Wick's theorem, see appendix, we get

$$a_p^\dagger a_q = \{a_p^\dagger a_q\} + \{\overbrace{a_p^\dagger a_q}\}$$

For particle states the contraction is equal to zero while for hole states it is equal to δ_{pq}.

$$\sum_{pq} \langle p| \hat{h} |q\rangle \, a_p^\dagger a_q = \sum_{pq} \langle p| \hat{h} |q\rangle \, \{a_p^\dagger a_q\} + \sum_i \langle i| \hat{h} |i\rangle$$

For the second term we need to normal order $\sum_{pqrs} a_p^\dagger a_q^\dagger a_s a_r$. With Wick's theorem the non-zero contractions are

$$\begin{aligned} a_p^\dagger a_q^\dagger a_s a_r = \; & \{a_p^\dagger a_q^\dagger a_s a_r\} + \{\overbrace{a_p^\dagger a_q^\dagger} a_s a_r\} + \{\overbrace{a_p^\dagger a_q^\dagger a_s} a_r\} + \{a_p^\dagger \overbrace{a_q^\dagger a_s} a_r\} \\ & + \{a_p^\dagger \overbrace{a_q^\dagger a_s a_r}\} + \{\overbrace{a_p^\dagger a_q^\dagger} a_s a_r\} + \{\overbrace{a_p^\dagger a_q^\dagger a_s} a_r\} \\ = \; & \{a_p^\dagger a_q^\dagger a_s a_r\} - \delta_{ips}\{a_q^\dagger a_r\} + \delta_{ipr}\{a_q^\dagger a_s\} \\ & + \delta_{iqs}\{a_p^\dagger a_r\} - \delta_{iqr}\{a_p^\dagger a_s\} - \delta_{ips}\delta_{jqr} + \delta_{ipr}\delta_{jqs} \end{aligned}$$

Again the contractions are equal to zero for particle states, but not for hole states. The interaction term then becomes

$$\begin{aligned} \sum_{pqrs} \langle pq| \hat{v} |rs\rangle \, a_p^\dagger a_q^\dagger a_s a_r = \; & \sum_{pqrs} \langle pq| \hat{v} |rs\rangle \, \{a_p^\dagger a_q^\dagger a_s a_r\} - \sum_{ipr} \langle iq| \hat{v} |ri\rangle \, \{a_q^\dagger a_r\} + \sum_{ips} \langle iq| \hat{v} |is\rangle \, \{a_q^\dagger a_s\} \\ & + \sum_{iqr} \langle pi| \hat{v} |ri\rangle \, \{a_p^\dagger a_r\} - \sum_{iqs} \langle pi| \hat{v} |is\rangle \, \{a_p^\dagger a_s\} \\ & - \sum_{ij} \langle ij| \hat{v} |ji\rangle + \sum_{ij} \langle ij| \hat{v} |ij\rangle \end{aligned}$$

Due to the anti symmetry $\langle pq| \hat{v} |rs\rangle = -\langle pq| \hat{v} |sr\rangle = -\langle qp| \hat{v} |rs\rangle = \langle qp| \hat{v} |sr\rangle$ this is

$$\begin{aligned} \sum_{pqrs} \langle pq| \hat{v} |rs\rangle \, a_p^\dagger a_q^\dagger a_s a_r = & \sum_{pqrs} \langle pq| \hat{v} |rs\rangle \, \{a_p^\dagger a_q^\dagger a_s a_r\} \\ & + 4 \sum_{ipq} \langle pi| \hat{v} |qi\rangle \, \{a_p^\dagger a_q\} + 2 \sum_{ij} \langle ij| \hat{v} |ij\rangle \end{aligned}$$

We can now write the Hamiltonian as

$$\begin{aligned} \hat{H} = & \sum_{pq} \langle p| \hat{h} |q\rangle \, \{a_p^\dagger a_q\} + \sum_{ipq} \langle pi| \hat{v} |qi\rangle \, \{a_p^\dagger a_q\} + \frac{1}{4} \sum_{pqrs} \langle pq| \hat{v} |rs\rangle \, \{a_p^\dagger a_q^\dagger a_s a_r\} \\ & + \sum_i \langle i| \hat{h} |i\rangle + \frac{1}{2} \sum_{ij} \langle ij| \hat{v} |ij\rangle \end{aligned} \tag{11}$$

or as

$$\hat{H} = \hat{H}_N + E_{ref} \tag{12}$$

with the normal ordered Hamiltonian defined as

$$\hat{H}_N = \sum_{pq} f_{pq}\{a_p^\dagger a_q\} + \frac{1}{4}\sum_{pqrs} \langle pq|\,\hat{v}\,|rs\rangle\,\{a_p^\dagger a_q^\dagger a_s a_r\} = \hat{F}_N + \hat{V}_N \tag{13}$$

and the reference energy

$$E_{ref} = \sum_i \langle i|\,\hat{h}\,|i\rangle + \frac{1}{2}\sum_{ij} \langle ij|\,\hat{v}\,|ij\rangle \tag{14}$$

In equation (13) we have also introduced a new variable

$$f_{pq} = \langle p|\,\hat{h}\,|q\rangle + \sum_i \langle pi|\,\hat{v}\,|qi\rangle \tag{15}$$

2.2 Paring model

A common way to model the nuclear structure is to assume that nucleons form pairs. This is supported by the fact that even-even nuclei are slightly more bound than odd-even and odd-odd nuclei[1]. More energy is needed to excite the nuclei since a pair has to be broken. Furthermore, the BCS theory of superconductivity assumes simultaneous creation and condensation of electron pairs, or Cooper pairs, due to electron-phonon interactions[2]. These realizations motivates the introduction of pairing interactions when studying certain many-body systems and their properties.
One such system is the simple pairing model of an ideal fermionic system where we assume no broken pairs, that is seniority quantum number $\mathcal{S} = 0$, [6] and spin degeneracy 2.

2.2.1 Hamiltonian

The pairing model Hamiltonian can be written on the form

$$\begin{aligned}\hat{H} =& \hat{H}_0 + \hat{H}_1 \\ =& \sum_p \epsilon_p a_p^\dagger a_p - \frac{1}{2} g \sum_{pq} a_{p+}^\dagger a_{p-}^\dagger a_{q-} a_{q+}\end{aligned} \tag{16}$$

where ϵ_p is the single-particle energy of level $p = 1, 2, \ldots$ and g is the pairing strength. Ideally the pairing strength can be treated as a constant, however for a realistic atomic nucleus this is not the case. Still it serves as a useful tool to study the pairing interaction. Assuming equally spaced single-particle orbitals by a constant ξ we can write $\epsilon_p = (p-1)\xi$, and introduce $\sigma = \pm$ representing the possible spin values. Next we recognize the number operator $\hat{n}_p = a_p^\dagger a_p$. The interaction part $\hat{H}_1$ can only excite a pair of particles at a time, so it is convenient to introduce the pair creation and annihilation operators $P_p^+ = a_{p+}^\dagger a_{p-}^\dagger$ and $P_p^- = a_{p-} a_{p+}$. This yields the simple expression:

$$\hat{H} = \xi \sum_{p\sigma} (p-1)\hat{n}_p - \frac{1}{2} g \sum_{pq} P_p^+ P_q^- \tag{17}$$

Since we are only dealing with pairs of particles occupying different energy levels, we can turn to occupation representation to calculate the matrix with Slater determinants as basis states. The basis will be composed of all possible variations of particle-hole excitations. The total number of basis states then becomes the binomial coefficient

$$\binom{p}{n} = \frac{p!}{n!(p-n)!} \tag{18}$$

where p is the number of hole states and n is the number of particle pairs. Since the particle pairs can not be broken we can define a general basis states in terms of pair creation and annihilation operators

$$\left|\Phi_{ij\ldots}^{ab\ldots}\right\rangle = P_a^+ P_b^+ \ldots P_k^- P_j^- P_i^- \left|\Phi_0\right\rangle \tag{19}$$

with the ground state defined as

$$\left|\Phi_0\right\rangle = \left(\prod_{i\leq F} P_i^\dagger\right)\left|0\right\rangle \tag{20}$$

acting on the vacuum state $|0\rangle$, where F denotes the Fermi level without degeneracy as we are exciting pairs. The matrix elements of equation (17) is given by

$$H_{ij} = \left\langle\phi_i\right|\hat{H}\left|\phi_j\right\rangle = \left\langle\phi_i\right|\hat{H}_0\left|\phi_j\right\rangle + \left\langle\phi_i\right|\hat{H}_1\left|\phi_j\right\rangle \tag{21}$$

for the any basis state $|\phi_i\rangle$. Lets first deal with the one-body part, given as

$$\left\langle\phi_i\right|\hat{H}_0\left|\phi_j\right\rangle = \xi\sum_{p\sigma}(p-1)\left\langle\phi_i\right|\hat{n}_{p\sigma}\left|\phi_j\right\rangle \tag{22}$$

where $\langle\phi_i|\hat{n}_{p\sigma}|\phi_j\rangle = \delta_{ij}$. Since only pairs will occupy a state we can substitute the sum over σ with 2. As the number operator acting on a state gives zero if no particle occupies that state ($a|0\rangle = 0$), we get

$$\left\langle\phi_i\right|\hat{H}_0\left|\phi_i\right\rangle = 2\xi\sum_{p}(p-1)\delta_{p\in\phi_i} \tag{23}$$

where the Kronecker delta $\delta_{p\in\phi_i}$ is zero unless state p is occupied in ϕ_i.
For the two-body part, we only get a contribution if there is a maximum of one pair different in the two slater deteminants. First we cover the diagonal elements:

$$\begin{aligned}
\left\langle\Phi_{ij\ldots}^{ab\ldots}\right|\hat{H}_1\left|\Phi_{ij\ldots}^{ab\ldots}\right\rangle &= -\frac{1}{2}g\sum_{pq}\left\langle\Phi_{ij\ldots}^{ab\ldots}\right|P_p^+P_q^-\left|\Phi_{ij\ldots}^{ab\ldots}\right\rangle \\
&= -\frac{1}{2}g\left[\sum_{pq>F}\delta_{pq}\sum_{c>F}\delta_{qc} + \sum_{pq<F}\delta_{pq}\sum_{k<F}^{F}\delta_{kq}\right] \\
&= -\frac{1}{2}g\left[\sum_{a>F}1 + \sum_{k<F}1\right] = -\frac{1}{4}g\cdot n_p
\end{aligned} \tag{24}$$

where $c \in \Phi_{ij\ldots}^{ab\cdots}$ and $k \in \Phi_{ij\ldots}^{ab\cdots}$. The off-diagonal elements will be

$$\left\langle \Phi_{ij\ldots}^{ab\cdots} \right| \hat{H}_1 \left| \Phi_{ij\ldots}^{ac\cdots} \right\rangle = -\frac{1}{2} g \sum_{pq} \delta_{pb} \delta_{qc} \tag{25}$$

for one different excited pair, and

$$\left\langle \Phi_{ij\ldots}^{ab\cdots} \right| \hat{H}_1 \left| \Phi_{ik\ldots}^{ab\cdots} \right\rangle = -\frac{1}{2} g \sum_{pq} \delta_{pj} \delta_{qk} \tag{26}$$

for one pair different under the fermi-level.

We have included a python script to calculate the hamiltonian for arbitrary number of pairs, basis states, ξ and g on our github.

2.3 Configuration Interaction[1]

We want to solve the time-independent Schröedinger Equation

$$\hat{H} \left| \Phi_k \right\rangle = (\hat{H}_0 + \hat{H}_1) \left| \Phi_k \right\rangle = \epsilon_k \left| \Phi_k \right\rangle \tag{27}$$

where we have written the Hamiltonian as a sum of one body and two body terms. The problem is that we do not know the solution when the particle-particle interaction is present. We do know however, that an arbitrary antisymmetric N-particle wave function can be written as a linear combination of Slater determinants. If we choose the K eigenfunctions Ψ_k of $\hat{H}_0$ as our basis, the solutions to equation (27) are then given by

$$\left| \Phi_k \right\rangle = c_0^{(k)} \left| \Psi_0 \right\rangle + \sum_{ia} c_i^{a(k)} \left| \Psi_i^a \right\rangle + \sum_{i<j, a<b} c_{ij}^{ab(k)} \left| \Psi_{ij}^{ab} \right\rangle + \cdots \tag{28}$$

We can write the Hamiltonian in the $\left|\Psi_i\right\rangle$ basis by utilizing the fact that $\sum_i \left|\Psi_i\right\rangle \left\langle\Psi_i\right| = I$:

$$\hat{H} = \sum_{ij} \left|\Psi_i\right\rangle \left\langle\Psi_i\right| \hat{H} \left|\Psi_j\right\rangle \left\langle\Psi_j\right| \tag{29}$$

By multiplying both sides with $\left\langle\Psi_l\right|$ and using equation (27) and (28), we see that

$$\left\langle\Psi_l\right| \hat{H} \left|\Phi_k\right\rangle = \sum_j \left\langle\Psi_l\right| \hat{H} \left|\Psi_j\right\rangle c_j = \epsilon_k c_l \tag{30}$$

This can be written in matrix notation as

$$\begin{bmatrix} \left\langle\Psi_0\right| \hat{H} \left|\Psi_0\right\rangle & \left\langle\Psi_0\right| \hat{H} \left|\Psi_1\right\rangle & \ldots & \left\langle\Psi_0\right| \hat{H} \left|\Psi_{\binom{K}{N}}\right\rangle \\ \left\langle\Psi_1\right| \hat{H} \left|\Psi_0\right\rangle & \left\langle\Psi_1\right| \hat{H} \left|\Psi_1\right\rangle & \ldots & \left\langle\Psi_1\right| \hat{H} \left|\Psi_{\binom{K}{N}}\right\rangle \\ \vdots & \vdots & \ddots & \vdots \\ \left\langle\Psi_{\binom{K}{N}}\right| \hat{H} \left|\Psi_0\right\rangle & \left\langle\Psi_{\binom{K}{N}}\right| \hat{H} \left|\Psi_1\right\rangle & \ldots & \left\langle\Psi_{\binom{K}{N}}\right| \hat{H} \left|\Psi_{\binom{K}{N}}\right\rangle \end{bmatrix} \begin{bmatrix} c_0 \\ c_1 \\ \vdots \\ c_{\binom{K}{N}} \end{bmatrix} = \epsilon_k \begin{bmatrix} c_0 \\ c_1 \\ \vdots \\ c_{\binom{K}{N}} \end{bmatrix} \tag{31}$$

[1] this section is copy-pasted from an earlier project, found at https://github.com/stiandb/ManyBodyFys4480/tree/master/PDF

Thus we can in principle solve equation (27) exactly by finding the eigenfunctions and eigenvalues of the above matrix. In practice however, w:e require an infinite number of single-particle wave functions to form a complete set, which means that the $\binom{K}{N}$ Slater determinants will not form a basis for our N-particle functions. Nevertheless, the solutions will be exact within the N-particle subspace spanned by our Slater determinants. From the number of Slater determinants, we can see how the problem scales with the number of particles N and basis functions K [5]:

$$\binom{K}{N} \approx \frac{16^{N/2}}{\pi N/2} \tag{32}$$

for large N. Hence, utilizing full configuration interaction can quickly become infeasible for large systems. In the next section we will therefore introduce another classical approximation method which scales better with the problem size.

2.4 Coupled Cluster Method

We start with the usual goal of approximating the exact solution of the time-independent Schrödinger equation for the ground state:

$$\hat{H} \left|\Psi\right\rangle = E \left|\Psi\right\rangle \tag{33}$$

given a system with normal-ordered Hamiltonian $\hat{H}$ and a wavefunction $\left|\Psi\right\rangle$. From equation (12) we are only interested in the contribution from the normal-ordered Hamiltonian

$$\hat{H}_N \left|\Psi\right\rangle = E_{CC} \left|\Psi\right\rangle \tag{34}$$

where E_{CC} is the correlation energy. In coupled cluster theory we have the ansatz for the ground state

$$\left|\Psi_{CC}\right\rangle = e^{\hat{T}} \left|\Phi_0\right\rangle \tag{35}$$

where $\left|\Phi_0\right\rangle$ is our reference vacuum and $\hat{T}$ is the cluster operator

$$\hat{T} = \hat{T}_1 + \hat{T}_2 + ... + \hat{T}_A \tag{36}$$

with A being the maximum number of particle-hole excitations, and

$$\hat{T}_n = \left(\frac{1}{n!}\right)^2 \sum_{ab...} \sum_{ij...} t_{ij...}^{ab...} a_a^\dagger a_b^\dagger \dots a_j a_i \tag{37}$$

where $ab\dots$ are states above and $ij\dots$ states below the Fermi level. The Schrödinger equation can then be written as

$$\hat{H}_N \left|\Psi_{CC}\right\rangle = E_{CC} \left|\Psi_{CC}\right\rangle \Leftrightarrow \hat{H}_N e^{\hat{T}} \left|\Phi_0\right\rangle = E_{CC} e^{\hat{T}} \left|\Phi_0\right\rangle \tag{38}$$

From this we can get an expression for the energy by left multiplying with $\left\langle\Phi_0\right| e^{-\hat{T}}$

$$E_{CC} = \left\langle\Phi_0\right| e^{-\hat{T}} \hat{H}_N e^{\hat{T}} \left|\Phi_0\right\rangle \tag{39}$$

where we can write the similarity transformed Hamiltonian $\bar{H} = e^{-\hat{T}}\hat{H}e^{\hat{T}}$. We can get a more intuitive expression for this by using the Baker-Campbell-Hausdorff expansion:

$$\bar{H} = \hat{H}_N + [\hat{H}_N, \hat{T}] + \frac{1}{2!}\left[[\hat{H}_N, \hat{T}], \hat{T}\right] + \dots \tag{40}$$

in many cases this will naturally truncate after a given number of terms, and so $\bar{H}$ can be computed exactly.

2.4.1 Coupled Cluster Doubles

A common practice is to truncate the cluster operator in equation (36) at $n = 2$ as this can account for a lot of the physics for some system. For this project, dealing with the pairing model, we will have to deal with the cluster operator $\hat{T} = \hat{T}_2$, since the pairing model only allows pair-excitations of particles. From equation (37) we get

$$\hat{T}_2 = \frac{1}{4}\sum_{abij} t_{ij}^{ab} a_a^\dagger a_b^\dagger a_j a_i \tag{41}$$

where t_{ij}^{ab} are the cluster amplitudes, which we have to find in order to calculate equation (38). The cluster operator will induce 2p-2h excitations and so, we can find the cluster amplitudes by calculating

$$\left\langle \Phi_{ij}^{ab} \right| \bar{H} \left| \Phi_0 \right\rangle = 0 \tag{42}$$

where

$$\left| \Phi_{ij}^{ab} \right\rangle = a_a^\dagger a_b^\dagger a_j a_i \left| \Phi_0 \right\rangle \tag{43}$$

To solve equation 42 we define

$$D_{ij}^{ab} = f_{ii} + f_{jj} - f_{aa} - f_{bb}$$

and subtract $D_{ij}^{ab} t_{ij}^{ab}$ from both sides of equation (42)

$$D_{ij}^{ab} t_{ij}^{ab} = D_{ij}^{ab} t_{ij}^{ab} + \left\langle \Phi_{ij}^{ab} \right| \bar{H} \left| \Phi_0 \right\rangle \tag{44}$$

Finally we divide both sides by D_{ij}^{ab} and end up with an iterative equation for the cluster amplitudes

$$t_{ij}^{ab} = t_{ij}^{ab} + \frac{\left\langle \Phi_{ij}^{ab} \right| \bar{H} \left| \Phi_0 \right\rangle}{D_{ij}^{ab}} \tag{45}$$

2.4.2 Matrix elements

Next we want to calculate the matrix elements of the similarity transformed Hamiltonian

$$\left\langle \Phi_0 \right| e^{-\hat{T}} \hat{H}_N e^{\hat{T}} \left| \Phi_0 \right\rangle = E_{CC} \tag{46}$$

$$\left\langle \Phi_{ij}^{ab} \right| e^{-\hat{T}} \hat{H}_N e^{\hat{T}} \left| \Phi_0 \right\rangle = 0 \tag{47}$$

To calculate these equations we will be using diagrams, we will elaborate more on this in the next section. Next we can rewrite the Baker-Campbell-Hausdorff expansion, equation (40), to our advantage. Since T only contains creation operators, we need H_N to contract these to get non-zero matrix elements. It turns out that the only non-zero terms in this expansion are the ones where the Hamiltonian has at least one contraction to every cluster operator on its right[3]. We can then write it as

$$e^{-\hat{T}}\hat{H}_N e^{\hat{T}} = \hat{H}_N + (\hat{H}_N\hat{T} + \frac{1}{2!}\hat{H}_N\hat{T}^2 + \dots)_C \tag{48}$$

where $()_C$ denotes that only terms where the Hamiltonian is connected to every cluster operator on its right are to be used. We find the correlation energy by combining equation 46 and equation (48) giving

$$E_{CC} = \langle\Phi_0|\,\hat{H}_N\,|\Phi_0\rangle + \langle\Phi_0|\,(\hat{H}_N\hat{T} + \frac{1}{2!}\hat{H}_N\hat{T}^2 + \dots)_C\,|\Phi_0\rangle \tag{49}$$

Obviously $\langle\Phi_0|\,\hat{H}_N\,|\Phi_0\rangle = 0$ because $\hat{H}_N$ is normal ordered, and as the Hamiltonian only can contract one cluster operator we are left with

$$E_{CC} = \langle\Phi_0|\,(\hat{H}_N\hat{T})_C\,|\Phi_0\rangle \tag{50}$$

Combining equation (47) and equation (48) gives

$$\left\langle\Phi_{ij}^{ab}\right|\hat{H}_N\,|\Phi_0\rangle + \left\langle\Phi_{ij}^{ab}\right|(\hat{H}_N\hat{T} + \frac{1}{2!}\hat{H}_N\hat{T}^2 + \dots)_C\,|\Phi_0\rangle = 0 \tag{51}$$

The expansion will truncate after T^2 as the Hamiltonian can only make up for one cluster operator, leaving us with the expression

$$\left\langle\Phi_{ij}^{ab}\right|\hat{H}_N\,|\Phi_0\rangle + \left\langle\Phi_{ij}^{ab}\right|(\hat{H}_N\hat{T})_C\,|\Phi_0\rangle + \frac{1}{2}\left\langle\Phi_{ij}^{ab}\right|(\hat{H}_N\hat{T}^2)_C\,|\Phi_0\rangle = 0 \tag{52}$$

Calculating all the contractions in this expression can be a tedious process. We simplify this with diagrams, see appendix B for theory and calculations, with the resulting expression

$$\begin{aligned}
\left\langle\Phi_{ij}^{ab}\right|\bar{H}\,|\Phi_0\rangle =& \langle ab|\,\hat{v}\,|ij\rangle + P(ab)\sum_c f_c^b t_{ij}^{ac} - P(ij)\sum_k f_j^k t_{ik}^{ab} \\
&+ \frac{1}{2}\sum_{cd}\langle ab|\,\hat{v}\,|cd\rangle\, t_{ij}^{cd} + \frac{1}{2}\sum_{kl}\langle kl|\,\hat{v}\,|ij\rangle\, t_{kl}^{ab} \\
&+ \frac{1}{2}P(ij)P(ab)\sum_{klcd}\langle kl|\,\hat{v}\,|cd\rangle\, t_{ik}^{ac}t_{lj}^{db} \\
&- \frac{1}{2}P(ij)\sum_{klcd}\langle kl|\,\hat{v}\,|cd\rangle\, t_{ki}^{cd}t_{lj}^{ab} \\
&+ \frac{1}{2}P(ab)\sum_{klcd}\langle kl|\,\hat{v}\,|cd\rangle\, t_{kl}^{ac}t_{ij}^{db} \\
&+ \frac{1}{4}\sum_{klcd}\langle kl|\,\hat{v}\,|cd\rangle\, t_{ij}^{cd}t_{kl}^{ab}
\end{aligned} \tag{53}$$

Unfortunatly this does not scale properly. In appendix C we make use of intermediates to get an efficient CCD implementation scaling as $\mathcal{O}(n_h^2 n_p^4)$. This is a significant improvement over FCI (see equation 32), but as we truncate at doubles excitations we are in many cases trading precision for speed.

We will now give a short introduction to the world of quantum computers before explaining a promising quantum algorithm for computing the FCI energies, namely the Quantum Phase Estimation Algorithm.

2.5 Quantum Computing

2.5.1 Basics

A bit is a basic unit of data in computation. In classical computers, a single bit has a binary value of either 1 or 0, and many bits can be assembled to represent complex information. For an n-bit classical computer, we are able to represent one of 2^n possible numbers at a time. The bits are manipulated by what is called logic gates to perform logical operations and their operation on bits can be used to perform complex tasks. In quantum computing on the other hand, we represent each bit (called a qubit) by the quantum state

$$|\psi\rangle = \alpha\,|0\rangle + \beta\,|1\rangle\,, \tag{54}$$

where we know from quantum mechanics that

$$\alpha^2 + \beta^2 = 1 \tag{55}$$

A qubit in this state is in what we call a superposition, where the value/state of the qubit is not determined before we measure it. The qubit will collapse to either of the states $|0\rangle$ or $|1\rangle$ upon measurement and the probability of the qubit collapsing to the state $|0\rangle$ is given by α^2 while it is given by β^2 for the state $|1\rangle$. Some of the magic of quantum computing comes from the fact that an n-qubit quantum computer can represent 2^n values/states at the same time:

$$\begin{aligned}(\alpha_1\,|0\rangle + \beta_1\,|1\rangle)(\alpha_2\,|0\rangle + \beta_2\,|1\rangle)\cdots(\alpha_n\,|0\rangle + \beta_n\,|1\rangle)\\ = \alpha_1\alpha_2\cdots\alpha_n\,|000\cdots0\rangle + \alpha_1\alpha_2\cdots\beta_n\,|000\cdots1\rangle + \cdots\\ = \sum_{i=0}^{2^n-1} a_i\,|i\rangle\end{aligned}$$

We can represent the states $|0\rangle$ and $|1\rangle$ with vectors which constructs a basis for $\mathbb{R}^2$;

$$\begin{aligned}|0\rangle &\equiv [1,0]^T\\ |1\rangle &\equiv [0,1]^T\end{aligned} \tag{56}$$

and use matrix algebra to represent manipulations on them. These matrices are a mathematical representation of what is called quantum gates and these gates have to preserve the probabilistic property given in equation (55). One can show that this property is preserved

when the matrices (which we will often refer to as operators from now on) are unitary. For an operator U, that is

$$U^\dagger U = UU^\dagger = I,$$

where I is the identity operator. We will switch between the braket- and vector notation in equation (56) when it suits our purpose.

Some of the most important single-qubit operators in quantum computing, and the ones most relevant to our project, are the Pauli gates;

$$\sigma_x = \begin{bmatrix} 0 & 1 \\ 1 & 0 \end{bmatrix} \qquad \sigma_y = \begin{bmatrix} 0 & -i \\ i & 0 \end{bmatrix} \qquad \sigma_z = \begin{bmatrix} 1 & 0 \\ 0 & -1 \end{bmatrix} \tag{57}$$

the Hadamard gate;

$$H = \frac{1}{\sqrt{2}} \begin{bmatrix} 1 & 1 \\ 1 & -1 \end{bmatrix} \tag{58}$$

and the rotation operators

$$R_n(\theta) = e^{-i\theta\sigma_n/2} = \cos\left(\frac{\theta}{2}\right) I - i \sin\left(\frac{\theta}{2}\right) \sigma_n \tag{59}$$

where $n \in \{x, y, z\}$. The Pauli X gate for example flips the qubit, that is

$$\sigma_x |0\rangle = \begin{bmatrix} 0 & 1 \\ 1 & 0 \end{bmatrix} \begin{bmatrix} 1 \\ 0 \end{bmatrix} = \begin{bmatrix} 0 \\ 1 \end{bmatrix} = |1\rangle \qquad \sigma_x |1\rangle = \begin{bmatrix} 0 & 1 \\ 1 & 0 \end{bmatrix} \begin{bmatrix} 0 \\ 1 \end{bmatrix} = \begin{bmatrix} 1 \\ 0 \end{bmatrix} = |0\rangle$$

while the Hadamard gate creates a superposition:

$$H |0\rangle = \frac{1}{\sqrt{2}} \begin{bmatrix} 1 & 1 \\ 1 & -1 \end{bmatrix} \begin{bmatrix} 1 \\ 0 \end{bmatrix} = \frac{1}{\sqrt{2}} \begin{bmatrix} 1 \\ 1 \end{bmatrix} = \frac{1}{\sqrt{2}} (|0\rangle + |1\rangle)$$
$$H |1\rangle = \frac{1}{\sqrt{2}} \begin{bmatrix} 1 & 1 \\ 1 & -1 \end{bmatrix} \begin{bmatrix} 0 \\ 1 \end{bmatrix} = \frac{1}{\sqrt{2}} \begin{bmatrix} 1 \\ -1 \end{bmatrix} = \frac{1}{\sqrt{2}} (|0\rangle - |1\rangle)$$

A gate that will become useful when we get into quantum fourier transform is the R_k gate:

$$R_k = \begin{bmatrix} 1 & 0 \\ 0 & e^{2\pi i/2^k} \end{bmatrix} \tag{60}$$

A system of multiple qubits are represented by tensor products. For example, for an n-qubit state we may write

$$|\psi_1\rangle |\psi_2\rangle \cdots |\psi_n\rangle \equiv |\psi_1\psi_2 \cdots \psi_n\rangle \equiv |\psi_1\rangle \otimes |\psi_2\rangle \otimes \cdots \otimes |\psi_n\rangle \tag{61}$$

We can also represent a manipulations on multiple qubits by a tensor product of operators;

$$(A \otimes B \otimes \cdots \otimes N) |\psi_1\rangle \otimes |\psi_2\rangle \otimes \cdots \otimes |\psi_n\rangle = A |\psi_1\rangle \otimes B |\psi_2\rangle \otimes \cdots \otimes N |\psi_n\rangle$$
$$or$$
$$A^1 B^2 \cdots N^n |\psi_1\rangle |\psi_2\rangle \cdots |\psi_n\rangle = A^1 |\psi_1\rangle B^2 |\psi_2\rangle \cdots N^n |\psi_n\rangle \tag{62}$$

where the superscript denotes which qubit the operator acts on. An important two-qubit gate is the CNOT-gate. Its matrix representation is given by

$$CNOT \equiv \begin{bmatrix} 1 & 0 & 0 & 0 \\ 0 & 1 & 0 & 0 \\ 0 & 0 & 0 & 1 \\ 0 & 0 & 1 & 0 \end{bmatrix} \tag{63}$$

Operating on two qubits $|c\rangle |t\rangle$, its task is to flip the target qubit $|t\rangle$ if the control qubit $|c\rangle$ is in the $|1\rangle$-state. If it is in the $|0\rangle$-state it should act as the identity operator. This kind of gate is called a controlled gate. In the case of the CNOT gate we perform a pauli-x gate on the target qubit conditioned on the control qubit, but we can of course apply any of the other gates mentioned.

2.5.2 Quantum Circuits

A convenient way to illustrate a quantum algorithm is through quantum circuits. A quantum cirquit consists of wires, where each wire represents a qubit:

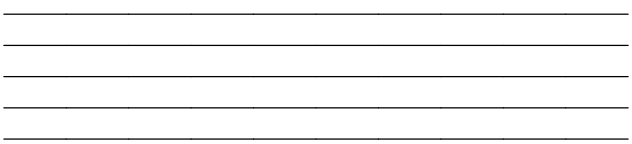

These wires are not physical wires, but you can think of them as representing the passage of time. When reading a quantum circuit, the leftmost operations are performed first, so the circuits are read from left to right. The qubits are usually initialized in the $|0\rangle$ state unless else is specified. To illustrate that an operation is perfomed on a qubit, we draw a gate on the wire corresponding to this qubit:

In the above circuit, we only have one qubit which is put in superposition by applying the hadamard gate (equation (58)). To illustrate conditional operations, like the CNOT gate, we write the circuit as follows:

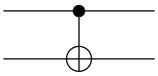

The black dot indicates that we put the condition on the first qubit, while the plus sign surrounded by a circle indicates which qubit to possibly apply the pauli-X gate on. We can also indicate conditional operations with an arbitrary gate A as follows:

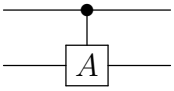

If we want to indicate that we perform a measurement on the bottom qubit in the circuit above, we can use a meter symbol on the wire corresponding to the qubit we measure:

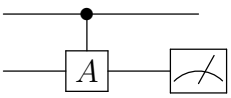

2.5.3 Quantum Fourier Transform

The Quantum Fourier Transform (QFT) is a linear transformation on qubits which is used quite frequently in quantum algorithms. The QFT performed on an orthonormal basis yields the following state:

$$|j\rangle \to \frac{1}{\sqrt{N}} \sum_{k=0}^{N-1} e^{2\pi ijk/N} |k\rangle \tag{64}$$

In order to see how we can implement this transformation on a quantum computer, we write the n-qubit state $|j\rangle$ using the binary representation $j = j_1 j_2 \cdots j_n$. Or

$$j = j_1 2^{n-1} + j_2 2^{n-2} + \cdots + j_n 2^0 \tag{65}$$

It is also useful to denote

$$0.j_1 j_2 \cdots j_n = j_1/2 + j_2/2^2 + \cdots + j_n/2^n, \tag{66}$$

as the binary fraction $0.j$. We can now rewrite equation (64):

$$\frac{1}{2^{n/2}} \sum_{k=0}^{2^n-1} e^{2\pi ijk/2^n} |k\rangle$$

Now use binary representation of k

$$= \frac{1}{2^{n/2}} \sum_{k_1=0}^{1} \cdots \sum_{k_n=0}^{1} e^{2\pi ij(\sum_{l=1}^{n} k_l 2^{n-l})/2^n)} |k_1 \cdots k_n\rangle$$

$$= \frac{1}{2^{n/2}} \sum_{k_1=0}^{1} \cdots \sum_{k_n=0}^{1} e^{2\pi ij(\sum_{l=1}^{n} k_l 2^{-l})} |k_1 \cdots k_n\rangle$$

$$= \frac{1}{2^{n/2}} \sum_{k_1=0}^{1} \cdots \sum_{k_n=0}^{1} \bigotimes_{l=1}^{n} e^{2\pi ijk_l 2^{-l}} |k_l\rangle$$

$$= \frac{1}{2^{n/2}} \bigotimes_{l=1}^{n} \sum_{k_l=0}^{1} e^{2\pi ijk_l 2^{-l}} |k_l\rangle$$

Insert $k_l = 0$ and $k_l = 1$

$$= \frac{1}{2^{n/2}} \bigotimes_{l=1}^{n} [|0\rangle + e^{2\pi ij2^{-l}} |1\rangle]$$

Now use the binary representation of j (eq. 65)

$$= \frac{1}{2^{n/2}} \bigotimes_{l=1}^{n} [|0\rangle + e^{2\pi i \sum_{i=1}^{n} j_i 2^{n-l-i}} |1\rangle]$$

Observe that when $k \geq 0$ for the terms $j_i 2^k$ in the exponent, we will just be multiplying $|1\rangle$ with 1. Therefore, we have

$$= \frac{1}{2^{n/2}} \left(|0\rangle + e^{2\pi i 0.j_n} |1\rangle\right) \left(|0\rangle + e^{2\pi i 0.j_{n-1} j_n} |1\rangle\right) \cdots \left(|0\rangle + e^{2\pi i 0.j_1 j_2 \cdots j_n} |1\rangle\right) \tag{67}$$

Let's see how we set up a circuit to perform a QFT on the state $|j_1 j_2 \cdots j_n\rangle$. First we apply a Hadamard gate to the first state:

$$H^1 |j_1 j_2 \cdots j_n\rangle = (|0\rangle + e^{2\pi i 0.j_1} |1\rangle) |j_2 \cdots j_n\rangle$$

We see that this expression is correct since $e^{2\pi i 0.j_1} = -1$ if $j_1 = 1$ and its 1 if $j_1 = 0$. For the next step, we need to apply a controlled R_2 gate to the first qubit, (see equation (60) for the R_k gate, with $k = 2$) conditioned on the second qubit. This action results in

$$(|0\rangle + e^{2\pi i 0.j_1 + 2\pi i j_2/2^2} |1\rangle) |j_2 \cdots j_n\rangle = (|0\rangle + e^{2\pi i 0.j_1 j_2} |1\rangle) |j_2 \cdots j_n\rangle$$

Continuing with applying a controlled R_k gate on the first qubit conditioned on qubit k for $k = 3, 4, ..., n$, we will end up with

$$(|0\rangle + e^{2\pi i 0.j_1 \cdots j_n} |1\rangle) |j_2 \cdots j_n\rangle$$

We can now apply the Hadamard gate to the second qubit and apply the controlled R_k gate on the preceeding qubits in the same manner and we will end up with equation (67). The complete circuit is illustrated below:

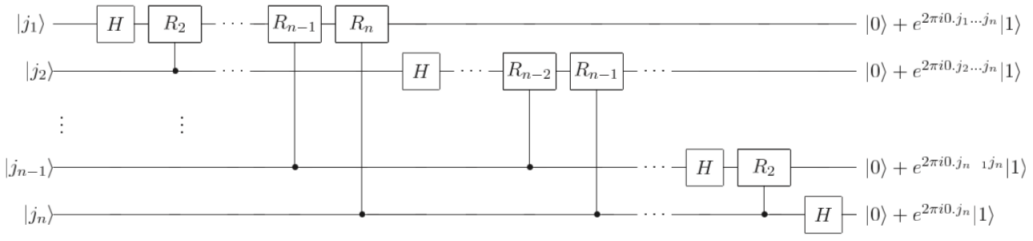

Figure 1: QFT circuit. Figure is taken from the book "Quantum computation and Quantum information" by Michael A. Nielsen and Isaac L. Chuang [9].

2.5.4 Quantum Phase Estimation

Now that we have shown how to do a Quantum Fourier transform, the next question one may ask is how to make use of it. A central procedure in many quantum algorithms is known as Phase Estimation. If we have a unitary operator U which has an eigenvector $|u\rangle$ with eigenvalue $e^{2\pi i \lambda}$, where λ is unknown, that is

$$U |u\rangle = e^{2\pi i \lambda} |u\rangle ,$$

the purpose of phase estimation is to estimate λ. The first stage of the phase estimation algorithm is shown in the figure below:

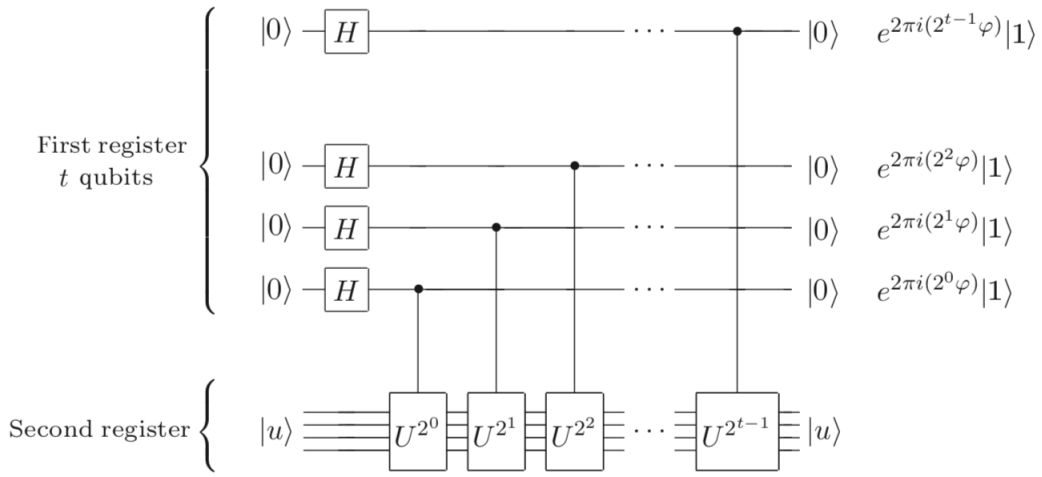

Figure 2: Phase estimation circuit. Figure is taken from the book "Quantum computation and Quantum information" by Michael A. Nielsen and Isaac L. Chuang [9].

What we see in figure (2) is that we have prepared two quantum registers. One with t qubits, all initialised in state $|0\rangle$ and the second register is initialized as the eigenvector $|u\rangle$. All the qubits in the first register is then put in a superposition by applying the Hadamard gate. We then apply the U^{2^0} operator to the second register, conditional on a qubit in the t-register. This yields

$$|u\rangle \frac{1}{2^{t/2}} \left(|0\rangle + e^{2\pi i 2^0 \lambda} |1\rangle\right) (|0\rangle + |1\rangle) \cdots (|0\rangle + |1\rangle)$$

Applying the U^{2^1} operator to the second register conditional on the next qubit in the t-register gives

$$|u\rangle \frac{1}{2^{t/2}} \left(|0\rangle + e^{2\pi i 2^0 \lambda} |1\rangle\right) \left(|0\rangle + e^{2\pi i 2^1 \lambda} |1\rangle\right) (|0\rangle + |1\rangle) \cdots (|0\rangle + |1\rangle).$$

Continuing as shown in the circuit gives us finally

$$|u\rangle \frac{1}{2^{t/2}} \left(|0\rangle + e^{2\pi i 2^0 \lambda} |1\rangle\right) \left(|0\rangle + e^{2\pi i 2^1 \lambda} |1\rangle\right) \left(|0\rangle + e^{2\pi i 2^2 \lambda} |1\rangle\right) \cdots \left(|0\rangle + e^{2\pi i 2^{t-1} \lambda} |1\rangle\right).$$

Note that an application of U^{2^p} doesn't require 2^p implementations of the operator U. Consider for example the rotation operator $[R_n(\theta)]^{2^p} = R_n(2^p\theta)$, and that all unitary operators can be written as a product of rotations ([9], pg. 175). We will make use of this property in our implementation.
Now suppose that we can write the phase exactly as the binary fraction

$$0.\lambda_1\lambda_2 \cdots \lambda_t = \lambda_1/2 + \lambda_2/2^2 + \cdots + \lambda_t/2^t.$$

The first qubit in the t-register can then be written as

$$|0\rangle + e^{2\pi i 2^0 \lambda} |1\rangle = |0\rangle + e^{2\pi i(\lambda_1/2 + \lambda_2/2^2 + \cdots + \lambda_t/2^t)} |1\rangle$$

$$= |0\rangle + e^{2\pi i 0.\lambda_1\lambda_2\cdots\lambda_t} |1\rangle$$

For the second qubit in the t-register, we can write

$$|0\rangle + e^{2\pi i 2^1\lambda} |1\rangle = |0\rangle + e^{2\pi i 2(\lambda_1/2+\lambda_2/2^2+\cdots+\lambda_t/2^t)} |1\rangle$$

Since λ_1 has to be either 1 or 0 we are then left with

$$|0\rangle + e^{2\pi i 2(\lambda_1/2+\lambda_2/2^2+\cdots+\lambda_t/2^t)} |1\rangle = |0\rangle + e^{2\pi i\lambda_1} e^{2\pi i(\lambda_2/2^1+\cdots+\lambda_t/2^{t-1})} |1\rangle$$

$$= |0\rangle + e^{2\pi i 0.\lambda_2\lambda_3\cdots\lambda_t} |1\rangle$$

Doing this for all the qubits in the t-register, we get

$$\frac{1}{2^{t/2}} \left(|0\rangle + e^{2\pi i 0.\lambda_1\cdots\lambda_t}\right) \left(|0\rangle + e^{2\pi i 0.\lambda_2\cdots\lambda_t}\right) \cdots \left(|0\rangle + e^{2\pi i 0.\lambda_t}\right) \tag{68}$$

Comparing this with the QFT equation (equation (67)), we see that they are of the same form. Since all operations on qubits are unitary, we can complex conjugate all the operations in the QFT circuit (figure (1)) to yield the inverse fourier transform. We can show this by considering some arbitrary unitary operations on a state $|j\rangle$:

$$ABCD\cdots N |j\rangle = |k\rangle$$

$$(ABCD\cdots N)^\dagger |k\rangle = (ABCD\cdots N)^\dagger ABCD\cdots N |j\rangle$$
$$= N^\dagger \cdots D^\dagger C^\dagger B^\dagger A^\dagger ABCD\cdots N |j\rangle = |j\rangle$$

By performing the inverse quantum fourier transform on the state in equation (68), we will end up with the state

$$|\lambda_1\lambda_2\cdots\lambda_t\rangle |u\rangle .$$

In other words, we get the exact phase. In reality though, we wont necessarily know the eigenvector $|u\rangle$. To deal with this, we can prepare the second register in a state $|\psi\rangle = \sum_{i=1}^{n} c_i |u_i\rangle$ which is a linear combination of the eigenstates. Repeated applications of the phase estimation algorithm followed by measurements will then yield a specter of eigenvalues and eigenvectors. We also cant always express the phase exactly as a t-bit binary fraction. It can be shown that we will with high probability produce a pretty good estimation to λ nevertheless ([9] section 5.2.1).

2.5.5 Hamiltonian Simulation

We know that a quantum state evolves according to the time evolution operator

$$|\psi(t)\rangle = e^{-i\hat{H}t/\hbar} |\psi(0)\rangle = \hat{U} |\psi(0)\rangle \tag{69}$$

We also know that an eigenstate of the Hamiltonian is an eigenstate of the time evolution operator. Its eigenvalue is given by

$$e^{-i\hat{H}t/\hbar} |\psi_k\rangle = e^{-iE_k t/\hbar} |\psi_k\rangle \tag{70}$$

where E_k is an eigenvalue of $\hat{H}$. On a quantum computer, the phase estimation algorithm finds the phase λ_k of a unitary operator with eigenvalue $e^{-i\lambda_k 2\pi}$. We know that the time evolution operator is unitary so if we can approximate this efficiently on a quantum computer, we can also approximate the eigenvalue of the Hamiltonian with the phase estimation algorithm. If our Hamiltonian $\hat{H}$ consists of several terms $\sum_k \hat{H}_k$, we can use the trotter approximation to rewrite $\hat{U}$ in a way that, as will be seen, is convenient to implement on a quantum computer. The trotter approximation is given by

$$e^{-i\sum_k \hat{H}_k t/\hbar} = \prod_k e^{-iH_k t/\hbar} + \mathcal{O}(t^2) \tag{71}$$

We first need to rewrite the pairing hamiltonian in terms of quantum logic gates. Some of the most notable are the Pauli gates, which are represented by the unitary matrices in equation (57). If we chose to represent a qubit in state $|0\rangle$ as a state with a fermion and $|1\rangle$ as a state with no fermion, we see that the operators

$$\begin{aligned} \sigma_+ &= \frac{1}{2}(\sigma_x + i\sigma_y) = \begin{bmatrix} 0 & 1 \\ 0 & 0 \end{bmatrix} \\ \sigma_- &= \frac{1}{2}(\sigma_x - i\sigma_y) = \begin{bmatrix} 0 & 0 \\ 1 & 0 \end{bmatrix}, \end{aligned} \tag{72}$$

has the following effect on qubits

$$\sigma_+ |1\rangle = |0\rangle \qquad \sigma_- |0\rangle = |1\rangle .$$

Hence σ_+ acts as a creation operator and σ_- acts as an annihilation operator. However, since fermionic states are anti-symmetric, $a_a^\dagger a_b^\dagger |c\rangle = -a_b^\dagger a_a^\dagger |c\rangle$, we need our quantum gate representation of the creation/annihilation operators to preserve this property. This can be achieved by multiplying the σ_z matrix on all the occupied states leading up to the one we operate on. The complete creation and annihilation operators can then be represented as

$$a_n^\dagger = \left(\prod_{k=1}^{n-1} \sigma_z^k\right) \sigma_+^n \qquad a_n = \left(\prod_{k=1}^{n-1} \sigma_z^k\right) \sigma_-^n \tag{73}$$

where the superscript tells us which qubit the operator acts on. For convenience, we chose that odd qubits are in a spin up state, while even qubits are in spin down state. For example for the following state

$$\begin{aligned} \textit{Qubit state:} &|0 \quad 0 \quad 1 \quad 1\rangle \\ \textit{Spin state:} &+ \quad - \quad + \quad - \\ \textit{Spacial state:} &\ 1 \quad 1 \quad 2 \quad 2 \end{aligned}$$

the first spacial basis state is occupied with an electron pair with opposite spin, while the second spacial state is not occupied. Our next job is to write our hamiltonian (equation (17)) in terms of the Pauli matrices and a detailed derivation is provided in the appendix section. Here we state the result: For the one body part of the hamiltonian we have the terms

$$\hat{H}_{0p} = \frac{1}{2}\delta(p - 1 - I[p\%2 = 0])(I^p + \sigma_z^p). \tag{74}$$

where we sum this term over each qubit p and % is the modulo operator.
$I[f(x) = y] = 1$ if $f(x) = y$ and zero otherwise. For the interaction term we have two possibilities. First for p = q we have:

$$\begin{aligned}\hat{V}_p = -\frac{1}{8}g\Big[&I^{\otimes 2p-2} \otimes I \otimes I \otimes I^{\otimes n-2p} \\ &+I^{\otimes 2p-2} \otimes I \otimes \sigma_z \otimes I^{\otimes n-2p} \\ &+I^{\otimes 2p-2} \otimes \sigma_z \otimes I \otimes I^{\otimes n-2p} \\ &+I^{\otimes 2p-2} \otimes \sigma_z \otimes \sigma_z \otimes I^{\otimes n-2p}\Big]\end{aligned} \tag{75}$$

and for $q - p \geq 1$ we get:

$$\begin{aligned}\hat{V}_{pq} = -\frac{1}{16}g[&I^{\otimes 2p-2} \otimes \sigma_x \otimes \sigma_x \otimes I^{\otimes 2(q-p-1)} \otimes \sigma_x \otimes \sigma_x \otimes I^{\otimes n-2q} \\ &- I^{\otimes 2p-2} \otimes \sigma_x \otimes \sigma_x \otimes I^{\otimes 2(q-p-1)} \otimes \sigma_y \otimes \sigma_y \otimes I^{\otimes n-2q} \\ &+ I^{\otimes 2p-2} \otimes \sigma_x \otimes \sigma_y \otimes I^{\otimes 2(q-p-1)} \otimes \sigma_x \otimes \sigma_y \otimes I^{\otimes n-2q} \\ &+ I^{\otimes 2p-2} \otimes \sigma_x \otimes \sigma_y \otimes I^{\otimes 2(q-p-1)} \otimes \sigma_y \otimes \sigma_x \otimes I^{\otimes n-2q} \\ &+ I^{\otimes 2p-2} \otimes \sigma_y \otimes \sigma_x \otimes I^{\otimes 2(q-p-1)} \otimes \sigma_x \otimes \sigma_y \otimes I^{\otimes n-2q} \\ &+ I^{\otimes 2p-2} \otimes \sigma_y \otimes \sigma_x \otimes I^{\otimes 2(q-p-1)} \otimes \sigma_y \otimes \sigma_x \otimes I^{\otimes n-2q} \\ &- I^{\otimes 2p-2} \otimes \sigma_y \otimes \sigma_y \otimes I^{\otimes 2(q-p-1)} \otimes \sigma_x \otimes \sigma_x \otimes I^{\otimes n-2q} \\ &+ I^{\otimes 2p-2} \otimes \sigma_y \otimes \sigma_y \otimes I^{\otimes 2(q-p-1)} \otimes \sigma_y \otimes \sigma_y \otimes I^{\otimes n-2q}]\end{aligned} \tag{76}$$

We have included a factor of two so the sum over p and q here can be restricted to $q > p$.

We then see that our complete pairing hamiltonian can be written as

$$\hat{H} = \sum_p \hat{H}_{0p} + \sum_p \hat{V}_p + \sum_{q>p} \hat{V}_{pq} \tag{77}$$

where $\hat{H}_{0p}$, $\hat{V}_p$ and $\hat{V}_{pq}$ is given by equation (74), (75) and (76) respectively. The time evolution operator is then given by

$$\hat{U}(t) = e^{-i(\sum_p \hat{H}_{0p} + \sum_p \hat{V}_p + \sum_{q>p} \hat{V}_{pq})t} \tag{78}$$

The trotter approximation (equation (71)) can now be used to approximate this operator. We get that

$$\hat{U}(t) = \prod_p e^{-i\hat{H}_{0p}t} \prod_p e^{-i\hat{V}_p t} \prod_{q>p} e^{-i\hat{V}_{pq}t} + \mathcal{O}(t^2) \tag{79}$$

We need a way to implement the above product on a quantum computer. To do this we utilize that a rotation of angle θ about axis $a \in \{x, y, z\}$ in the block sphere is given by

$$R_a(\theta) = e^{-i\frac{\theta}{2}\sigma_a} = cos(\frac{\theta}{2})I - isin(\frac{\theta}{2})\sigma_a. \tag{80}$$

Further we have that

$$\sigma_x = H\sigma_z H \tag{81}$$

and

$$\sigma_y = R_z(\pi/2)H\sigma_z H R_z(-\pi/2) \tag{82}$$

and also that the following circuit implements the time evolution $e^{-i\sigma_z\otimes\sigma_z\otimes\sigma_z\otimes\sigma_z\Delta t} =$

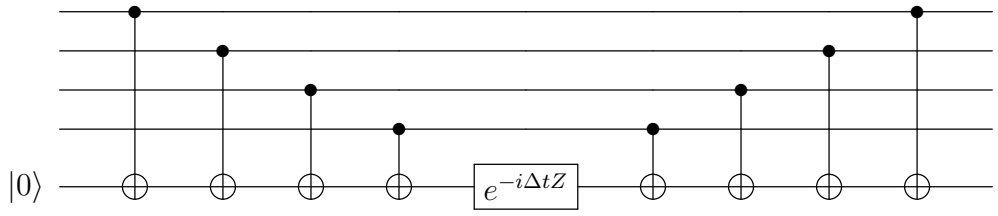

We see that equation (80), (81), (82) and this circuit is all we need to implement the products in the pairing time evolution operator. For example, for the tensor product $H = \sigma_x \otimes \sigma_y \otimes \sigma_x \otimes \sigma_y$ we have:

$$\begin{aligned}
&H \otimes R_z(\pi/2)H \otimes H \otimes R_z(\pi/2)H \\
&\times e^{-i\Delta t\sigma_z\otimes\sigma_z\otimes\sigma_z\otimes\sigma_z} \\
&\times H \otimes HR_z(-\pi/2) \otimes H \otimes HR_z(-\pi/2) \\
&= U e^{-i\Delta t\sigma_z\otimes\sigma_z\otimes\sigma_z\otimes\sigma_z} U^\dagger \\
&= U[cos(\Delta t)I - isin(\Delta t)\sigma_z \otimes \sigma_z \otimes \sigma_z \otimes \sigma_z]U^\dagger \\
&= cos(\Delta t)I - isin(\Delta t)\sigma_x \otimes \sigma_y \otimes \sigma_x \otimes \sigma_y \\
&= e^{-i\Delta t\sigma_x\otimes\sigma_y\otimes\sigma_x\otimes\sigma_y}
\end{aligned}$$

since $UU^\dagger = I$ and

$$\begin{aligned}
&U \times (\sigma_z \otimes \sigma_z \otimes \sigma_z \otimes \sigma_z) \times U^\dagger \\
&= (H \otimes R_z(\pi/2)H \otimes H \otimes R_z(\pi/2)H) \\
&\times(\sigma_z \otimes \sigma_z \otimes \sigma_z \otimes \sigma_z) \\
&\times(H \otimes HR_z(-\pi/2) \otimes H \otimes HR_z(-\pi/2)) \\
&= H\sigma_z H \otimes R_z(\pi/2)H\sigma_z HR_z(-\pi/2) \otimes H\sigma_z H \otimes R_z(\pi/2)H\sigma_z HR_z(-\pi/2) \\
&= \sigma_x \otimes \sigma_y \otimes \sigma_x \otimes \sigma_y
\end{aligned}$$

2.5.6 Practical information on the Phase Estimation implementation

The phase estimation algorithm is aimed at finding λ_k for a unitary operator $\hat{U}$ with eigenvalue $e^{i2\pi\lambda_k}$, such that

$$\hat{U}\left|\psi_k\right\rangle = e^{i2\pi\lambda_k}\left|\psi_k\right\rangle,$$

In our case, the time evolution operator has the eigenvalues $e^{-iE_k\Delta t}$ which means that the value we read from the phase estimation algorithm is

$$\lambda_k = -E_k\Delta t/2\pi$$

An assumption with the phase estimation algorithm is that we can write the eigenvalue $\lambda = 0.\lambda_1\lambda_2\cdots\lambda_t$ as a binary fraction. Since this is a positive number less than one, we need our eigenvalues to be negative for the phase estimation algorithm to work according to the above equation for λ_k. We can force this by subtracting a large enough constant value E_{max} from the Hamiltonian since

$$(\hat{H} - E_{max})\left|\phi_k\right\rangle = (E_k - E_{max})\left|\phi_k\right\rangle.$$

This gives us

$$\lambda_k = -(E_k - E_{max})\Delta t/2\pi$$
$$\lambda_k 2\pi/\Delta t = E_{max} - E_k$$
$$E_k = E_{max} - \lambda_k 2\pi/\Delta t$$

Further, since the phase estimation algorithm yields the following state for the work qubits

$$\left|\lambda_1\lambda_2\cdots\lambda_t\right\rangle = \left|\lambda 2^t\right\rangle$$

we transform the measured binary number to a binary fraction before plugging it into the equation for E_k. We can also see that if we have $\lambda = \lambda^{'} + n > 1$ where $0 < \lambda^{'} < 1$ and n is a positive integer, we get from the phase estimation algorithm

$$e^{i2\pi(\lambda^{'}+n)} = e^{i2\pi n}e^{i2\pi\lambda^{'}} = e^{i2\pi\lambda^{'}}$$

or written in binary form

$$e^{i2\pi(\lambda^{'}+n)} = e^{i2\pi\lambda_1\cdots\lambda_k.\lambda_{k+1}\cdots\lambda_n} = e^{i2\pi 0.\lambda_{k+1}\cdots\lambda_n}$$

In other words; for eigenvalues greater than one, we lose information. A restriction on $\lambda_k < 1$ gives

$$-E_k\Delta t/2\pi < 1$$
$$\implies -E_k\Delta t < 2\pi$$

or

$$-(E_k - E_{max})\Delta t < 2\pi$$

Substituting E_k with E_{min} (the lowest eigenvalue of $\hat{H}$) gives the upper bound on Δt in order to yield the whole eigenvalue spectrum

$$\Delta t < \frac{2\pi}{E_{max} - E_{min}}$$

We also have to keep in mind the number of work qubits to use. k work qubits gives us the ability to represent 2^k binary fractions. A quantum state represented by s simulation qubits potentially has 2^s eigenvalues. This means that we will have $\frac{2^t}{2^s} = 2^{t-s}$ points for each eigenvalue. Section 5.4.2 in the article in ref [10] illustrates that a surplus of around 5 work qubits are usually sufficient to calculate the eigenvalue-spectra.

3 Results

3.1 Phase estimation

We run the phase estimation algorithm on the unitary operator given by equation (79). We do this with four simulation qubits and for varying amount of work qubits. The simulation qubits are initialised to superpositions of bell states since electron pairs are not allowed to be separated. We perform 1000 measurements on the system. ξ and g from equation (17) was both set to 1. The results can be seen in the plots in figure (3) below:

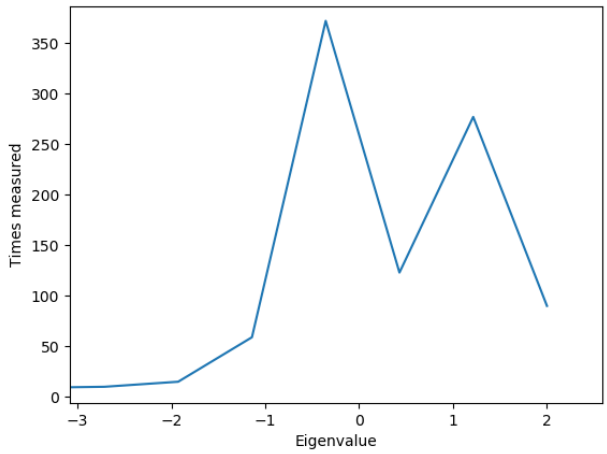

(a) 4 simulation and 4 work qubits

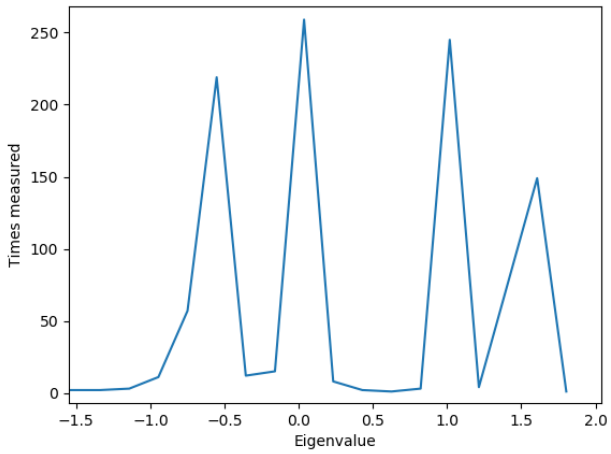

(b) 4 simulation and 6 work qubits

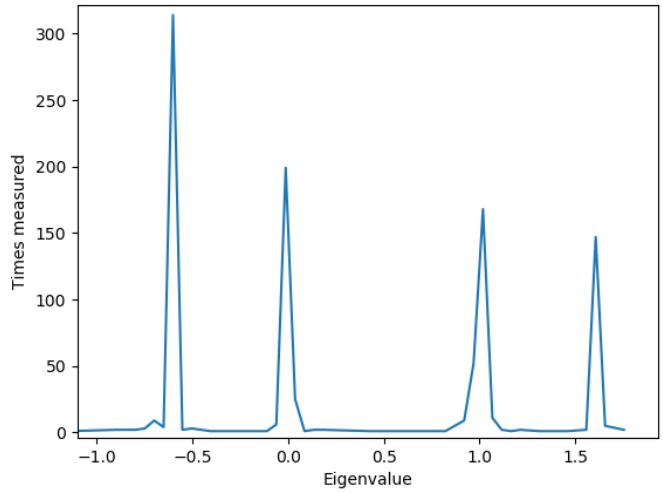

(c) 4 simulation and 8 work qubits

Figure 3: Plots of the amount of times an eigenvalue estimate is measured against the eigenvalue estimate. The quantum circuit is run and measured 1000 times in total.

We see that as we increase the amount of work qubits, we get well defined peaks in the

distribution of the measured eigenvalues. We can find the eigenvalues from the plots by approximating eigenvalue j with the mean of peak j as

$$E[\lambda^{(j)}] = \frac{\sum_i \lambda_i^{(j)} N_i^{(j)}}{\sum_i N_i^{(j)}}$$

where $\lambda_i^{(j)}$ is the i'th measurement in peak j and $N_i^{(j)}$ is the number of times its measured. The variance is then given by

$$\frac{1}{\sum_i N_i^{(j)}} \sum_i (E[\lambda^{(j)}] - \lambda_i^{(j)})^2.$$

In order to do this, we need to define a minimum amount of measurements before the algorithm considers that an eigenvalue to belongs to a peak. We set this value to 4 measurements and the results for 8 work qubits can be can be seen in table 1 below:

Number of pairs	FCI Eigenvalue(s)	Quantum Eigenvalue(s)
0	0	0.0 ± 0.2
1	$-0.61803399, \quad 1.61803399$	$-0.6 \pm 0.1, \quad 1.61 \pm 0.06$
2	1.00000000	1.0 ± 0.2

Table 1: FCI and quantum computer energies for 4 basis states for one and two pairs. $\xi = 1$, $g = 1$. We also provide two standard deviations with the quantum phase estimation algorithm.

We see that the FCI and Quantum phase estimation eigenvalues correspond well.
We also ran the same quantum algorithm, but this time with added measurement and gate noise. The properties which specify the amount of noise is gathered from IBMs real quantum computer, named Melbourne. The results can be seen in figure (4) below:

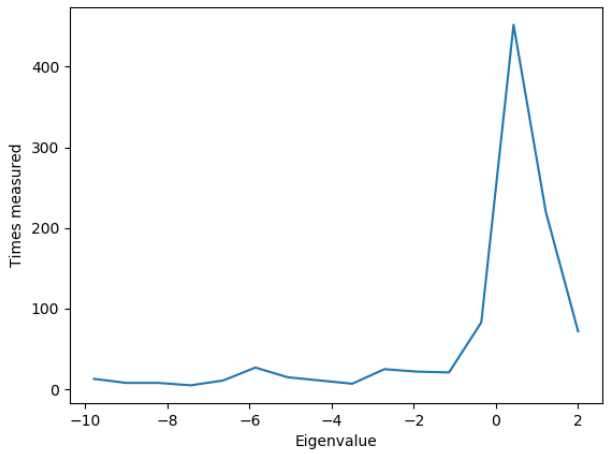

(a) 4 simulation and 4 work qubits

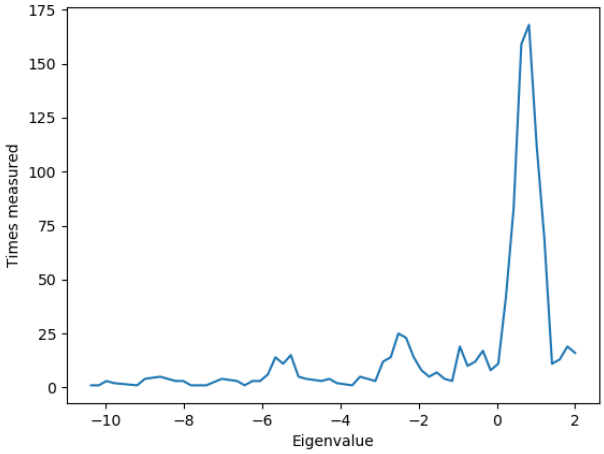

(b) 4 simulation and 6 work qubits

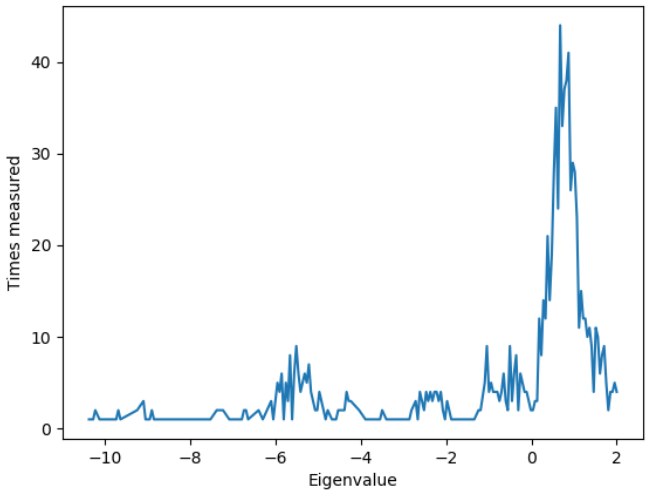

(c) 4 simulation and 8 work qubits

Figure 4: Plots of the amount of times an eigenvalue estimate is measured against the eigenvalue estimate. The quantum circuit is run and measured 1000 times in total. We have added measurement and gate noise which is extracted from IBM's real quantum computer "Melbourne"

As we can see, the addition of measurement and gate noise made the quantum phase estimation algorithm unable to locate the eigenvalues of our system.

3.2 Coupled cluster doubles

The CCD calculations are done for two and four particles with a fixed level spacing $\xi = 1$ and varying interaction strength g. Figure (5) show the results benchmarked against FCI

calculations for three different numbers of spin orbitals.

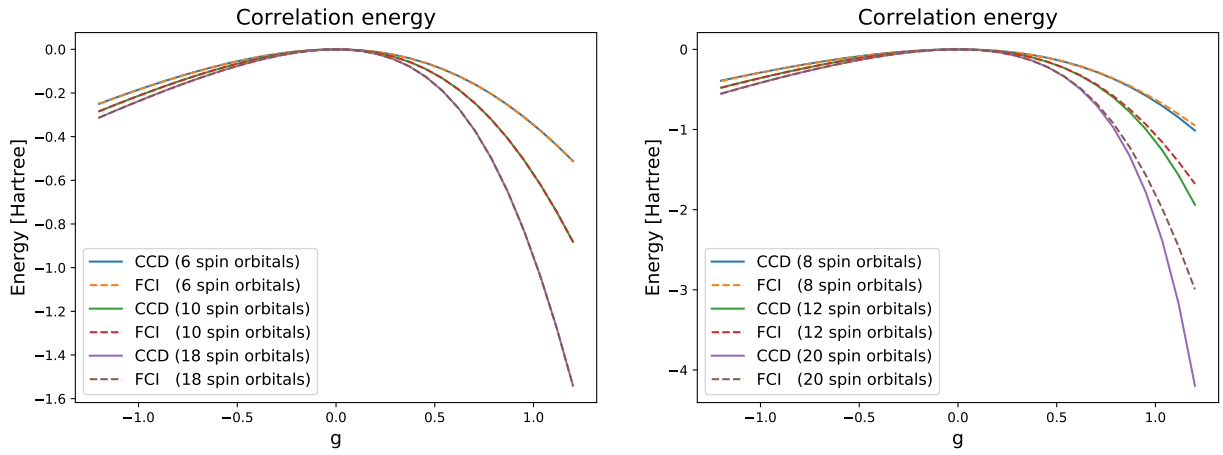

(a) Two particles.

(b) Four particle.

Figure 5: CCD and FCI calculations of pairing model with fixed level spacing $\xi = 1$ and varying pairing interaction.

For both systems the correlation energy is negative, thus they correspond to a bound state. We see that for a two-particle system CCD is equivalent to FCI. The difference is only dependent on the convergence restriction in the CCD-code, here set to 10^{-10}. For the four-particle system we see a divergence from CCD and FCI as the interaction strength increases in magnitude.
Next we show the ground state energy for an increasing number of spin orbitals. Again the results are benchmarked against FCI calculations, as shown in figure (6), with $\xi = 1$ and $g = 1$. We do this for four particles only since FCI and CCD are equivalent for two particles.

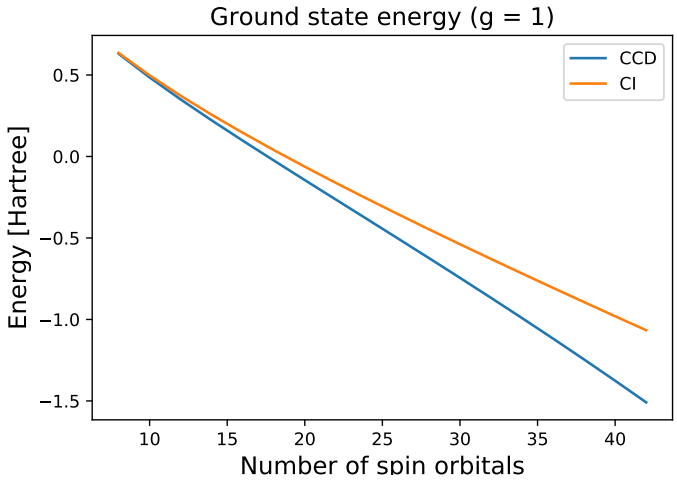

Figure 6: Ground state energy of pairing model with an increasing number of spin orbitals. Fixed level spacing $\xi = 1$ and interaction strength $g = 1$.

4 Discussion

First off, we examined the eigenvalues found with the phase estimation algorithm. As we can see from figure 3, we get defined peaks in the distribution of measurements as we increase the number of work qubits. This is expected as t work qubits can represent 2^t binary numbers, yielding a doubling of the resolution with a unit increase of t. Further we found, as can be seen in table 1, that the quantum phase estimation algorithm yielded eigenvalues within two standard deviations of the eigenvalues found with configuration interaction theory. We used the same amount of spacial basis states in both methods and since FCI yields an exact result within the basis spanned by these states, it serves as a good benchmark for the quantum algorithm. Further we see that while we need to specify the amount of pairs for the FCI algorithm, the quantum algorithm provides the eigenvalues for all possible amount of pairs (in the case of 4 simulation qubits; 0, 1 and 2 pairs). From the same analysis, but with added measurement and gate noise (figure 4) we get an indication that publicly available Quantum computers today struggle with the phase estimation algorithm due to noise. There are quantum algorithms, namely Variational Quantum Eigensolvers [12], which are regarded as less susceptible to noise and also more likely to work on a near term device. We would like to do the same type of analysis for this algorithm in the near future. Further, we used the trotter approximation to order $\mathcal{O}(t^2)$, but it would be interesting to compare this with the approximation to order $\mathcal{O}(t^3)$. Research have indicated that while the $\mathcal{O}(t^3)$ approximation requires roughly twice as many operations per iteration, the decrease in the required amount of iterations provides a reduction in computational time when compared with the $\mathcal{O}(t^2)$ approximation ([10] pg. 83).

In order to compare a well known and efficient classical algorithm with phase estimation, we implemented Coupled Cluster Doubles (CCD). We compared the correlation energy with the one obtained from FCI. For two particles we see that CCD is equivalent to FCI, see figure 5a. This is because all possible excitation coefficients are induced by the coupled cluster ansatz, and we get the exact solution in the space spanned by a given number of spin orbitals. We discuss this in more detail in appendix D. Here we also state that this is the only case where CCD is exact, as it can tweak all $2p-2h$ coefficients, t_{ij}^{ab}. For an n-particle system there are possible $np-nh$ excitations. This is supported by the four-particle results where CCD diverges from FCI with an increasing number of spin orbitals, see figure 5b. However, in equation (48) we simplified the Baker-Campbell-Hausdorff expansion using that only terms where the Hamiltonian has at least one contraction to every cluster operator on its right give non-zero terms. The expansion will then truncate naturally at $\hat{H}_N\hat{T}^4$, but these terms are not included in the doubles approximation and a quadruples approximation is needed. As the single and triple cluster amplitudes is zero in terms of the pairing model, a quadruples approximation would not include too many extra terms and should not be difficult to derive by hand. This would serve as a good extension to this project in the future. Figure 6 shows how the energy approximation from CCD diverges FCI as the number of spin orbitals increases. This could be explained by the fact that even though we are able to excite two pairs with the operator $\hat{T}_2^2$, the contributions will be decided by a product of doubles amplitudes $t_{ij}^{ab}t_{kl}^{cd}$, unlike FCI where we have a specific amplitude for each spin orbital in our basis (see equation 28). Thus FCI provides more degrees of freedom than CCD and we see

that even though CCD is efficient, it could lack contributions important for the system.

5 Conclusion

The quantum algorithm provided results which showed good correspondence with the eigenvalues provided with FCI. As can be seen in table 1, we got the eigenvalues -0.6 ± 0.1 and 1.61 ± 0.06 for one pair, and this result is consistent with the FCI eigenvalues -0.618 and 1.618. For two pairs, the quantum algorithm yielded 1.0 ± 0.2 which also is consistent with the FCI eigenvalue of 1.0. We also found that an increase in the amount of work qubits provided a higher resolution in the estimate of the eigenvalues as expected. With measurement and gate noise added to the quantum simulation, we were unable to extract the eigenvalues from our measurements and this is a limiting factor for the application of this algorithm on current devices. We utilized the trotter approximation to order $\mathcal{O}(t^2)$ and it would be interesting to compare this approximation with the approximation to order $\mathcal{O}(t^3)$.

The coupled cluster doubles approximation provided exact results compared to FCI for two particles, but failed to give sufficient results for more particles and a growing number of spatial orbitals.

For future work, we would have liked to apply phase estimation to an increasing number of spin orbitals and varying interaction strength to provide a more direct comparison with CCD. Unfortunately, the simulation was to time consuming. However, as we can see from the right hand side of figure 5b, CCD doesnt keep up with FCI when we are dealing with eight spin orbitals and four particles, whereas the phase estimation algorithm provided the correct eigenvalue within two standard deviations for the same system (see table 1 under 2 pairs). We would also want to compare our noisy phase estimation results with that of an variational quantum eigensolver.

References

[1] A. Bohr, B. R. Mottelson, and D. Pines. Possible analogy between the excitation spectra of nuclei and those of the superconducting metallic state. *Phys. Rev.*, 110:936–938, May 1958.

[2] Leon N. Cooper. Bound electron pairs in a degenerate fermi gas. *Phys. Rev.*, 104:1189–1190, Nov 1956.

[3] T. Daniel Crawford and Henry F. Schaefer III. An introduction to coupled cluster theory for computational chemists. In *Reviews in Computational Chemistry*, pages 33–136. John Wiley Sons, Ltd, 2007.

[4] David Deutch. Quantum theory, the church-turing principle and the universal quantum computer. 1985.

[5] T. Helgaker, P. Jorgensen, and J. Olsen. *Molecular Electronic-structure Theory*. Wiley, 2008.

[6] Morten H. Jensen and D. J. Dean. Pairing in nuclear systems: from neutron stars to finite nuclei. *journals.aps.org*, April 2003.

[7] Tomi H Johnson. What is a quantum simulator? 2014.

[8] Seth Lloyd. Universal quantum simulators. 1996.

[9] Michael A. Nielsen and Isaac L. Chuang. Quantum computation and quantum information. Mai 2003.

[10] Eirik Ovrum. Quantum computing and many-body physics. Mai 2003.

[11] Rigetti. Noise and quantum computation. 2019.

[12] Jonathan Romero, Ryan Babbush, Jarrod R. McClean, Cornelius Hempel, Peter Love, and Alán Aspuru-Guzik. Strategies for quantum computing molecular energies using the unitary coupled cluster ansatz, 2017.

[13] Isaiah Shavitt and Rodney J. Bartlett. Many-body methods in chemistry and physics: Mbpt and coupled-cluster theory. pages 297–308. 2009.

Appendix A: Hamiltonian to Pauli matrices

Here we show how we write our hamiltonian (eq:Hamiltonian) in terms of the Pauli matrices. First, we observe that

$$\begin{aligned} a_i^\dagger a_i &= \left(\prod_{k=1}^{i-1}\sigma_z^k\right)\sigma_+^i\left(\prod_{k=1}^{i-1}\sigma_z^k\right)\sigma_-^i \\ &= \sigma_+^i\sigma_-^i = \frac{1}{2}(I^i+\sigma_z^i) \end{aligned}$$

and see that the one-body part of the hamiltonian can be written as

$$\hat{H}_0 = \frac{1}{2}\xi\sum_p([(p-1)-(p-1)\%2]/2)(I^p+\sigma_z^p).$$

where p now runs over each qubit and $\%$ is the modulo operator. Now for the interaction term:

$$\begin{aligned} &\hat{V} = \\ &-\frac{1}{2}g\sum_{pq}\left(\prod_{k=1}^{2p-2}\sigma_z^k\right)\sigma_+^{2p-1}\left(\prod_{k=1}^{2p-1}\sigma_z^k\right)\sigma_+^{2p}\left(\prod_{k=1}^{2q-1}\sigma_z^k\right)\sigma_-^{2q}\left(\prod_{k=1}^{2q-2}\sigma_z^k\right)\sigma_-^{2q-1} \end{aligned} \tag{A.1}$$

We can see that

$$\begin{aligned} \left(\prod_{k=1}^{2p-2}\sigma_z^k\right)\sigma_+^{2p-1}\left(\prod_{k=1}^{2p-1}\sigma_z^k\right)\sigma_+^{2p} = \\ \sigma_z^{\otimes^{2p-2}}\otimes\sigma_+\otimes I^{\otimes^{n-2p-1}}\times\sigma_z^{\otimes^{2p-1}}\otimes\sigma_+\otimes I^{\otimes^{n-2p}} = \\ I^{\otimes^{2p-2}}\otimes\sigma_+\sigma_z\otimes\sigma_+\otimes I^{\otimes^{n-2p}} \end{aligned}$$

so we can rewrite equation (A.1) as

$$\begin{aligned} &\hat{V} = \\ &-\frac{1}{2}g\sum_{pq}\left[I^{\otimes^{2p-2}}\otimes\sigma_+\otimes\sigma_+\otimes I^{\otimes^{n-2p}}\right]\left[I^{\otimes^{2q-2}}\otimes\sigma_-\otimes\sigma_-\otimes I^{\otimes^{n-2q}}\right] \end{aligned}$$

We have two possibilities here. First for $p=q$:

$$-\frac{1}{2}g\left[I^{\otimes^{2p-2}}\otimes\sigma_+\sigma_-\otimes\sigma_+\sigma_-\otimes I^{\otimes^{n-2p}}\right] \tag{A.2}$$

and for $q-p\geq 1$ we have

$$-\frac{1}{2}g\left[I^{\otimes^{2p-2}}\otimes\sigma_+\otimes\sigma_+\otimes I^{\otimes^{2(q-p-1)}}\otimes\sigma_-\otimes\sigma_-\otimes I^{\otimes^{n-2q}}\right] \tag{A.3}$$

For $p-q \geq 1$ we simply exchange p with q and σ_+ with σ_-. To continue, we insert the expressions for $\sigma_\pm$ (equation (72)) into these equations. For p = q (equation (A.2)) we then have:

$$\begin{aligned} V_{p=q} &= -\frac{1}{8}g\Big[I^{\otimes^{2p-2}} \otimes (I+\sigma_z) \otimes (I+\sigma_z) \otimes I^{\otimes^{n-2p}}\Big] \\ &= -\frac{1}{8}g\Big[I^{\otimes^{2p-2}} \otimes I \otimes I \otimes I^{\otimes^{n-2p}} \\ &\quad + I^{\otimes^{2p-2}} \otimes I \otimes \sigma_z \otimes I^{\otimes^{n-2p}} \\ &\quad + I^{\otimes^{2p-2}} \otimes \sigma_z \otimes I \otimes I^{\otimes^{n-2p}} \\ &\quad + I^{\otimes^{2p-2}} \otimes \sigma_z \otimes \sigma_z \otimes I^{\otimes^{n-2p}}\Big] \end{aligned}$$

and for $q-p \geq 1$ (equation (A.3)) we get:

$$-\frac{1}{32}g\left[I^{\otimes^{2p-2}} \otimes (\sigma_x + i\sigma_y) \otimes (\sigma_x + i\sigma_y) \otimes I^{\otimes^{2(q-p-1)}} \otimes (\sigma_x - i\sigma_y) \otimes (\sigma_x - i\sigma_y) \otimes I^{\otimes^{n-2q}}\right]$$

This can be rewritten as sixteen four qubit operations

$$\begin{aligned} -\frac{1}{32}g[&I^{\otimes^{2p_q-2}} \otimes \sigma_x \otimes \sigma_x \otimes I^{\otimes^{2(q_p-p_q-1)}} \otimes \sigma_x \otimes \sigma_x \otimes I^{\otimes^{n-2q_p}} \\ &\mp iI^{\otimes^{2p_q-2}} \otimes \sigma_x \otimes \sigma_x \otimes I^{\otimes^{2(q_p-p_q-1)}} \otimes \sigma_x \otimes \sigma_y \otimes I^{\otimes^{n-2q_p}} \\ &\mp iI^{\otimes^{2p_q-2}} \otimes \sigma_x \otimes \sigma_x \otimes I^{\otimes^{2(q_p-p_q-1)}} \otimes \sigma_y \otimes \sigma_x \otimes I^{\otimes^{n-2q_p}} \\ &- I^{\otimes^{2p_q-2}} \otimes \sigma_x \otimes \sigma_x \otimes I^{\otimes^{2(q_p-p_q-1)}} \otimes \sigma_y \otimes \sigma_y \otimes I^{\otimes^{n-2q_p}} \\ &\pm iI^{\otimes^{2p_q-2}} \otimes \sigma_x \otimes \sigma_y \otimes I^{\otimes^{2(q_p-p_q-1)}} \sigma_x \otimes \sigma_x \otimes I^{\otimes^{n-2q_p}} \\ &+ I^{\otimes^{2p_q-2}} \otimes \sigma_x \otimes \sigma_y \otimes I^{\otimes^{2(q_p-p_q-1)}} \otimes \sigma_x \otimes \sigma_y \otimes I^{\otimes^{n-2q_p}} \\ &+ I^{\otimes^{2p_q-2}} \otimes \sigma_x \otimes \sigma_y \otimes I^{\otimes^{2(q_p-p_q-1)}} \otimes \sigma_y \otimes \sigma_x \otimes I^{\otimes^{n-2q_p}} \\ &\mp iI^{\otimes^{2p_q-2}} \otimes \sigma_x \otimes \sigma_y \otimes I^{\otimes^{2(q_p-p_q-1)}} \otimes \sigma_y \otimes \sigma_y \otimes I^{\otimes^{n-2q_p}} \\ &\pm iI^{\otimes^{2p_q-2}} \otimes \sigma_y \otimes \sigma_x \otimes I^{\otimes^{2(q_p-p_q-1)}} \otimes \sigma_x \otimes \sigma_x \otimes I^{\otimes^{n-2q_p}} \\ &+ I^{\otimes^{2p_q-2}} \otimes \sigma_y \otimes \sigma_x \otimes I^{\otimes^{2(q_p-p_q-1)}} \otimes \sigma_x \otimes \sigma_y \otimes I^{\otimes^{n-2q_p}} \\ &+ I^{\otimes^{2p_q-2}} \otimes \sigma_y \otimes \sigma_x \otimes I^{\otimes^{2(q_p-p_q-1)}} \otimes \sigma_y \otimes \sigma_x \otimes I^{\otimes^{n-2q_p}} \\ &\mp iI^{\otimes^{2p_q-2}} \otimes \sigma_y \otimes \sigma_x \otimes I^{\otimes^{2(q_p-p_q-1)}} \otimes \sigma_y \otimes \sigma_y \otimes I^{\otimes^{n-2q_p}} \\ &- I^{\otimes^{2p_q-2}} \otimes \sigma_y \otimes \sigma_y \otimes I^{\otimes^{2(q_p-p_q-1)}} \otimes \sigma_x \otimes \sigma_x \otimes I^{\otimes^{n-2q_p}} \\ &\pm iI^{\otimes^{2p_q-2}} \otimes \sigma_y \otimes \sigma_y \otimes I^{\otimes^{2(q_p-p_q-1)}} \otimes \sigma_x \otimes \sigma_y \otimes I^{\otimes^{n-2q_p}} \\ &\pm iI^{\otimes^{2p_q-2}} \otimes \sigma_y \otimes \sigma_y \otimes I^{\otimes^{2(q_p-p_q-1)}} \otimes \sigma_y \otimes \sigma_x \otimes I^{\otimes^{n-2q_p}} \\ &+ I^{\otimes^{2p_q-2}} \otimes \sigma_y \otimes \sigma_y \otimes I^{\otimes^{2(q_p-p_q-1)}} \otimes \sigma_y \otimes \sigma_y \otimes I^{\otimes^{n-2q_p}}] \end{aligned}$$

where the subscript is used if $p > q$. We can easily see that when running over the sum over p and q, the terms with $\pm$ and $\mp$ sign in front will cancel out. Also, we can include a factor 2 and limit the sum to $p < q$. Therefore:

$$
\begin{aligned}
V_{p\neq q} = -\frac{1}{16} g[& I^{\otimes^{2p-2}} \otimes \sigma_x \otimes \sigma_x \otimes I^{\otimes^{2(q-p-1)}} \otimes \sigma_x \otimes \sigma_x \otimes I^{\otimes^{n-2q}} \\
& - I^{\otimes^{2p-2}} \otimes \sigma_x \otimes \sigma_x \otimes I^{\otimes^{2(q-p-1)}} \otimes \sigma_y \otimes \sigma_y \otimes I^{\otimes^{n-2q}} \\
& + I^{\otimes^{2p-2}} \otimes \sigma_x \otimes \sigma_y \otimes I^{\otimes^{2(q-p-1)}} \otimes \sigma_x \otimes \sigma_y \otimes I^{\otimes^{n-2q}} \\
& + I^{\otimes^{2p-2}} \otimes \sigma_x \otimes \sigma_y \otimes I^{\otimes^{2(q-p-1)}} \otimes \sigma_y \otimes \sigma_x \otimes I^{\otimes^{n-2q}} \\
& + I^{\otimes^{2p-2}} \otimes \sigma_y \otimes \sigma_x \otimes I^{\otimes^{2(q-p-1)}} \otimes \sigma_x \otimes \sigma_y \otimes I^{\otimes^{n-2q}} \\
& + I^{\otimes^{2p-2}} \otimes \sigma_y \otimes \sigma_x \otimes I^{\otimes^{2(q-p-1)}} \otimes \sigma_y \otimes \sigma_x \otimes I^{\otimes^{n-2q}} \\
& - I^{\otimes^{2p-2}} \otimes \sigma_y \otimes \sigma_y \otimes I^{\otimes^{2(q-p-1)}} \otimes \sigma_x \otimes \sigma_x \otimes I^{\otimes^{n-2q}} \\
& + I^{\otimes^{2p-2}} \otimes \sigma_y \otimes \sigma_y \otimes I^{\otimes^{2(q-p-1)}} \otimes \sigma_y \otimes \sigma_y \otimes I^{\otimes^{n-2q}}]
\end{aligned}
$$

Appendix B: Diagrams

In many cases the often messy and long process of contracting operators can be simplified by using Goldstone diagrams. The reference state is represented by empty space and lines represent orbitals that differ from this. Upward arrows represent particle lines, and downward arrows represent hole lines. Components of the Hamiltonian are indicated with a horizontal dashed line, while components of the cluster operator is indicated with a horizontal solid line. We will take advantage of the following rules for the mathematical expression corresponding to a diagram:

- With every interaction vertex is an associated expectation value:
  - One-body interactions: $\langle \text{out} | \, \hat{h} \, | \text{in} \rangle$
  - Two-body interactions: $\langle \text{out left, out right} | \, \hat{v} \, | \text{in left, in right} \rangle$
- With every $\hat{T}$ vertex is an associated amplitude t.
- The sign is $(-1)^{h+l}$, where h is the number of hole lines and l is the number of loops.
- Sum over all internal indices, that is lines that are connected in both ends.
- Multiply with a factor of $\frac{1}{2}$ for each pair of lines that connect the two same vertices in the same direction.
- Multiply with a factor of $\frac{1}{2}$ for each pair of equivalent vertices.
- To ensure antisymmetry, sum over all unique permutations of unconnected lines on different vertices.
- Ignore disconnected terms, as they will cancel each other out.

B.1 Diagrammatic representation of the matrix elements

Since we are dealing with the pairing model, we have to make sure that particle pairs are not broken. For the two-body operator

$$V_N = \frac{1}{4}\sum_{pqrs} \langle pq|\,\hat{v}\,|rs\rangle\,\{a_p^\dagger a_q^\dagger a_s a_r\} \tag{B.1}$$

the only states that give non-zero matrix elements without breaking any particle pairs are $|ij\rangle$ and $|ab\rangle$. Thus, we only have to consider $\langle ab|\,\hat{v}\,|cd\rangle$, $\langle ij|\,\hat{v}\,|kl\rangle$, $\langle ab|\,\hat{v}\,|ij\rangle$ and $\langle kl|\,\hat{v}\,|cd\rangle$ represented as diagrams below

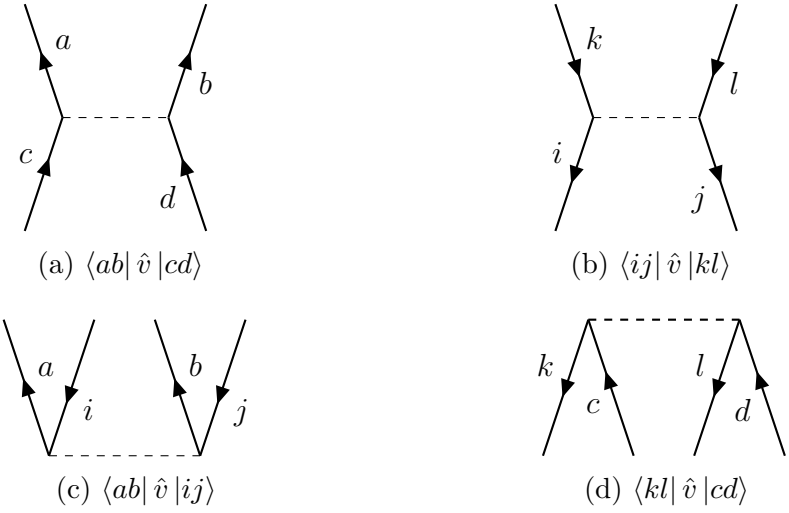

(a) $\langle ab|\,\hat{v}\,|cd\rangle$ (b) $\langle ij|\,\hat{v}\,|kl\rangle$

(c) $\langle ab|\,\hat{v}\,|ij\rangle$ (d) $\langle kl|\,\hat{v}\,|cd\rangle$

Figure 7: Possible two-body diagrams of the Hamiltonian

For the one-body operator

$$F_N = \sum_{pq}\left(\,\langle p|\,\hat{h}\,|q\rangle + \sum_i \langle pi|\,\hat{v}\,|qi\rangle\,\right)\{a_p^\dagger a_q\} \tag{B.2}$$

we get non-zero contributions for all $p = q$ in the first term and all $p, q = j$ in the second term. In other words we only have to consider f_a^b and f_i^j, represented as diagrams below

(a) f_a^b (b) f_i^j

Figure 8: Possible one-body diagrams of the Hamiltonian

The cluster operator in equation (41) is represented by

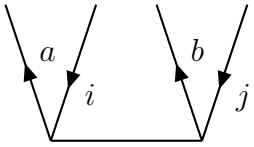

Figure 9: Diagram for cluster operator $\hat{T}_2$

To solve equation (50 - 52) we want all diagrams connecting the cluster operator to the one-body or two-body diagrams. For the energy we only want fully connected diagrams to get non-zero values. Clearly the only diagram satisfying this is

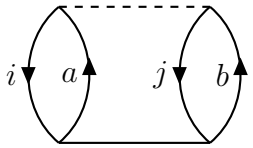

Figure 10: Diagram for the energy

with two downward lines, two loops and two pairs of lines connecting in the same direction giving the equation

$$E_{CC} = \frac{1}{4} \sum_{ijab} \langle ij| \hat{v} |ab\rangle \, t_{ij}^{ab} \tag{B.3}$$

To solve equation (52) we want open lines for i, j, a, b to get non-zero values. Looking at figure (7) the only diagram inducing the correct excitation for the first term is (c). For the second term we need to connect T and H_N with the correct excitation. A careful observation will reveal that for both (a) and (b) in figure (7) and (a) and (b) in figure (8) this can only happen in one way. Finding the topologically unique diagrams is a bit more difficult for the third term than for the others as there are multiple equivalent diagrams that can be made. There is a method developed by Bartlett[13] to solve this problem efficiently. We assign a $+$ symbols to particle lines and a $-$ symbols to hole lines. Lines with the same sign can connect, and the different ways to connect these diagrams will represent the topologically different diagrams.

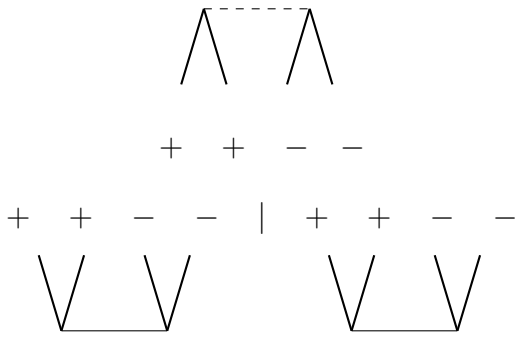

Following this we find that the possible combinations for the last term in equation (52) are

$$++|--\quad -|++-\quad +|+--\quad +-|+-$$

where their symmetric counterpart is equivalent. We are then left with all the possible diagrams for equation (52) listed in figure (12). Here we have made certain changes to diagram (g), corresponding to $-|++-$ to get a better looking diagram using the antisymmetry of the cluster amplitudes.

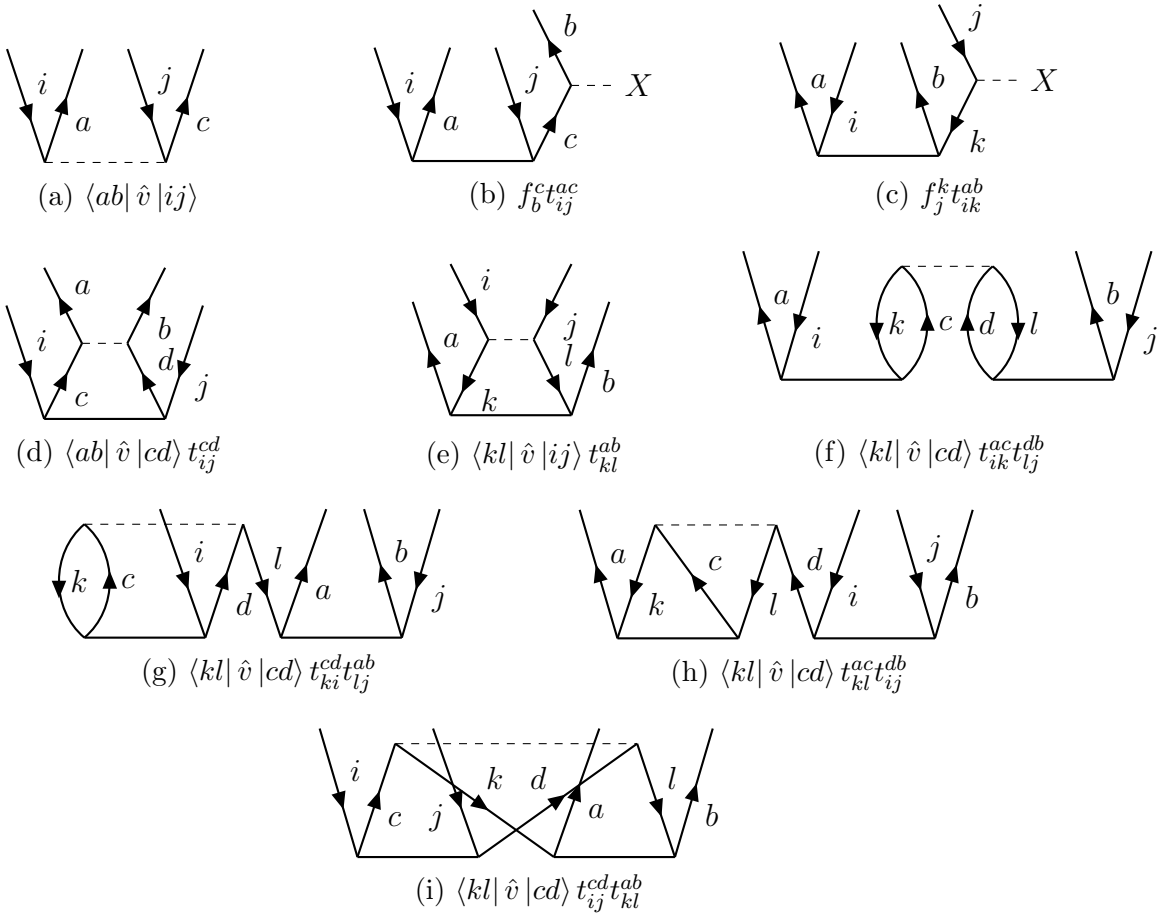

Figure 12: Diagrams for the H_{ij}^{ab} amplitudes.

B.2 Analytical expressions

To find the expressions corresponding to the diagrams in figure (12) we will make use of the rules defined earlier in this section. We see that all diagrams except (c) and (g) has an even number of hole lines and loops, thus these are the only ones with a corresponding negative expression. Next we see possible permutations of particle lines on different vertices in diagram (b), (e), (f) and (h), as well as possible permutations of hole lines in diagram (c), (d), (f) and (g). Furthermore, diagram (f) - (i) contain two equivalent vertices being the cluster vertices, and diagram (i) also has a pair of lines connecting the two same vertices in

the same direction. This yield the expression for the expectation value

$$\begin{aligned}\left\langle \Phi_{ij}^{ab}\right| \bar{H} \left|\Phi_0\right\rangle = &\left\langle ab\right| \hat{v} \left|ij\right\rangle + P(ab)\sum_c f_c^b t_{ij}^{ac} - P(ij)\sum_k f_j^k t_{ik}^{ab} \\ &+ \frac{1}{2}\sum_{cd} \left\langle ab\right| \hat{v} \left|cd\right\rangle t_{ij}^{cd} + \frac{1}{2}\sum_{kl} \left\langle kl\right| \hat{v} \left|ij\right\rangle t_{kl}^{ab} \\ &+ \frac{1}{2}P(ij)P(ab)\sum_{klcd} \left\langle kl\right| \hat{v} \left|cd\right\rangle t_{ik}^{ac} t_{lj}^{db} \\ &- \frac{1}{2}P(ij)\sum_{klcd} \left\langle kl\right| \hat{v} \left|cd\right\rangle t_{ki}^{cd} t_{lj}^{ab} \\ &+ \frac{1}{2}P(ab)\sum_{klcd} \left\langle kl\right| \hat{v} \left|cd\right\rangle t_{kl}^{ac} t_{ij}^{db} \\ &+ \frac{1}{4}\sum_{klcd} \left\langle kl\right| \hat{v} \left|cd\right\rangle t_{ij}^{cd} t_{kl}^{ab}\end{aligned} \tag{B.4}$$

Appendix C: Efficient implementation of CCD code

A naive implementation of the coupled cluster equations will not result in the expected efficiency associated with the coupled cluster method. Here we list certain changes that will improve this.

C.1 Interaction channels

To solve equation (B.4) we first need to calculate and store the matrix elements $\sum_{pq} f_q^p$ and $\sum_{pqrs} \left\langle pq\right| \hat{v} \left|rs\right\rangle$. For systems with many single-particle states these matrices will grow large. This will reduce the performance of our algorithm in terms of both speed and storage. If we were to calculate all the elements of the matrices we would need a lot of memory available. However, as most of the elements always are zero, we mention this briefly in section (B) where $\left\langle ai\right| \hat{v} \left|bj\right\rangle = 0$ and $f_i^a = 0$, we do not need to store these. Instead we can divide them into different channels that run over indices that can give non-zero elements. These will be the same as the diagrams in figure (7) and figure (8): $\sum_{ab} f_a^b$, $\sum_{ij} f_i^j$, $\sum_{abcd} \left\langle ab\right| \hat{v} \left|cd\right\rangle$, $\sum_{ijkl} \left\langle ij\right| \hat{v} \left|kl\right\rangle$ and $\sum_{abij} \left\langle ab\right| \hat{v} \left|ij\right\rangle$.

C.2 Intermediates

Next we notice that some terms in equation (B.4) scales badly. The most notable terms are the ones summing over four variables, that scales as $\mathcal{O}(n_h^4 n_p^4)$. We improve this by defining the intermediates

$$\chi_{ijkl} = \sum_{cd} \left\langle kl\right| \hat{v} \left|cd\right\rangle t_{ij}^{cd} \tag{C.1}$$

$$\chi_{il} = -\sum_{kcd} \left\langle kl\right| \hat{v} \left|cd\right\rangle t_{ki}^{cd} \tag{C.2}$$

$$\chi_{ad} = \sum_{klc} \langle kl| \hat{v} |cd\rangle \, t_{kl}^{ac} \tag{C.3}$$

$$\chi_{bcjk} = \sum_{ld} \langle kl| \hat{v} |cd\rangle \, t_{lj}^{db} \tag{C.4}$$

factorizing the four last terms. We see that the most expensive computation scales as $\mathcal{O}(n_h^3 n_p^3)$. Combining this with equation (B.4) we get

$$\begin{aligned} \left\langle \Phi_{ij}^{ab} \right| \bar{H} \left| \Phi_0 \right\rangle = \langle ab| \hat{v} |ij\rangle &+ P(ab) \sum_c f_c^b t_{ij}^{ac} - P(ij) \sum_k f_j^k t_{ik}^{ab} \\ &+ \frac{1}{2} \sum_{cd} \langle ab| \hat{v} |cd\rangle \, t_{ij}^{cd} + \frac{1}{2} \sum_{kl} \langle kl| \hat{v} |ij\rangle \, t_{kl}^{ab} \\ &+ \frac{1}{2} P(ij) P(ab) \sum_{ck} \chi_{bcjk} t_{ik}^{ac} + \frac{1}{2} P(ij) \sum_l \chi_{il} t_{lj}^{ab} \\ &+ \frac{1}{2} P(ab) \sum_d \chi_{ad} t_{ij}^{db} + \frac{1}{4} \sum_{kl} \chi_{ijkl} t_{kl}^{ab} \end{aligned} \tag{C.5}$$

that now scales as $\mathcal{O}(n_h^2 n_p^4)$.

C.3 Iterative mixing

Iterative solvers can sometimes run into oscillating solutions. One simple way to fix this to introduce iterative mixing when updating the cluster amplitudes in equation (45).

$$t^{new'} = \alpha t^{new} + (1 - \alpha) t^{old} \tag{C.6}$$

Appendix D: Transition amplitudes

Here we discuss the difference between CCD and FCI in terms of parameters, stating why they are equivalent for two particles and not for four particles. We know that FCI is exact within the space spanned by a given number of spin orbitals, with parameters corresponding to all possible excitations, see equation (28). Coupled cluster on the other hand defines a truncated space for which we hope contains the exact solution. The full coupled cluster ansatz yield

$$e^{\hat{T}} \left| \Phi_0 \right\rangle = (1 + \hat{T} + \frac{\hat{T}^2}{2} + \frac{\hat{T}^3}{3!} + \dots) \left| \Phi_0 \right\rangle \tag{D.1}$$

For coupled cluster doubles we have

$$\left| \Phi_{CCD} \right\rangle = (1 + \hat{T}_2 + \frac{\hat{T}_2^2}{2} + \frac{\hat{T}_2^3}{3!} + \dots) \left| \Phi_0 \right\rangle \tag{D.2}$$

and in terms of the cluster amplitudes

$$\left| \Phi_{CCD} \right\rangle = \left| \Phi_0 \right\rangle + \sum_{ijab} t_{ij}^{ab} \left| \Phi_{ij}^{ab} \right\rangle + \frac{1}{2} \sum_{\substack{ijab \\ klcd}} t_{ij}^{ab} t_{kl}^{cd} \left| \Phi_{ijkl}^{abcd} \right\rangle + \dots \tag{D.3}$$

The full configuration interaction for the same excitations yield

$$|\Phi_{FCI}\rangle = c_0 |\Phi_0\rangle + \sum_{ijab} c_{ij}^{ab} \left|\Phi_{ij}^{ab}\right\rangle + \sum_{\substack{ijab \\ klcd}} c_{ijkl}^{abcd} \left|\Phi_{ijkl}^{abcd}\right\rangle + \dots \tag{D.4}$$

Here the coupled cluster parameters are dependent of the truncation, and so deals with a lower number of parameters than FCI for the same system. This can be seen in the last term of both equations, where FCI have independent $4p - 4h$ parameters and CCD have parameters consisting of $2p - 2h$ parameters. From this we can argue that FCI will yield better results within the same basis as it operates with more degrees of freedom than CCD. In addition the number of parameters scale with both the number of particles and the number of spin orbitals.